Imaging mesoscopic spin Hall flow: Spatial distribution of local spin currents and spin densities in and out of multiterminal spin-orbit coupled semiconductor nanostructures

Branislav K. Nikolić, Liviu P. Zârbo, and Satofumi Souma*
Department of Physics and Astronomy, University of Delaware, Newark, Delaware 19716-2570, USA
(Received 27 July 2005; revised manuscript received 12 December 2005; published 2 February 2006)

We introduce the concept of *bond spin currents*, which describe the spin transport between two sites of the lattice model of a multiterminal spin-orbit (SO) coupled semiconductor nanostructure, and express them in terms of the spin-dependent nonequilibrium (Keldysh) Green functions for the Landauer setup where the nanostructure is attached to many semi-infinite ideal leads terminating in macroscopic thermalizing reservoirs. This formalism is applied to obtain the spatial distribution of microscopic spin currents in a *clean* phase-coherent two-dimensional electron (2DEG) gas with the Rashba type of SO coupling attached to four external leads. Together with the corresponding spatial profiles of the steady-state spin density, such visualization of the phase-coherent spin flow allow us to resolve several key issues for the understanding of microscopic mechanisms which generate pure spin Hall currents in the transverse leads of ballistic devices due to the flow of unpolarized charge current through their longitudinal leads: (i) while bond spin currents are nonzero locally within the SO coupled sample and neighboring region of the leads even in equilibrium (when all leads are at the same potential), the *total* spin currents obtained by summing the bond spin currents over any cross section within the leads are zero, so that no spin is actually transported by such equilibrium spin currents; (ii) when the device is brought into a nonequilibrium state (supporting steady-state charge current) by applying the external voltage difference between its longitudinal leads, only the wave functions (or Green functions) around the Fermi energy contribute to the total spin current through a given transverse cross section; (iii) the total spin Hall current is not conserved within the SO coupled region—however, it becomes conserved and physically well-defined quantity in the ideal leads where it is, furthermore, equal to the spin current obtained within the multiprobe Landauer-Büttiker scattering formalism in linear response regime. The spatial profiles of the local spin currents and stationary flowing spin densities crucially depend on whether the sample is smaller or greater than the *spin precession length*, thereby demonstrating its essential role as the characteristic mesoscale for the spin Hall effect in ballistic multiterminal semiconductor nanostructures. Although the static spin-independent disorder reduces the magnitude of the total spin current in the leads, the bond spin currents and spin densities remain nonzero throughout the whole diffusive 2DEG sample.

DOI: 10.1103/PhysRevB.73.075303 PACS number(s): 72.10.Bg, 73.23.−b, 72.25.Dc, 71.70.Ej

I. INTRODUCTION

The recent experimental observation of the spin Hall effect[1,2] has opened new avenues for the understanding of the fundamental role which spin-orbit (SO) couplings[3,4] can play in transport and equilibrium properties of semiconductor structures. While SO coupling effects are tiny relativistic corrections for particles moving through electric fields in vacuum, they can be enhanced in solids by several orders of magnitude due to the interplay of crystal symmetry and strong crystalline potential.[3,4] Furthermore, harnessing of spin currents induced by the spin Hall effect offers new possibilities for the envisioned all-electrical manipulation of spin for semiconductor spintronics applications[5] where electrical fields can access individual spins on short length and time scales.

The principal phenomenological manifestation of the spin Hall effect is unique: the transverse spin current, which is pure in the sense of not being accompanied by any net charge transport in the transverse direction, emerges as the response to conventional unpolarized charge current in the longitudinal direction through a paramagnetic system in the absence of any external magnetic field. When such current hits the sample boundary, it will deposit nonequilibrium spin accumulation[6–10] at the lateral edges of the sample attached to two longitudinal electrodes,[9,10] as detected optically in recent breakthrough experiments.[1,2]

However, there are several apparently disconnected mechanisms capable of inducing the spin Hall currents. Nonetheless, they share the necessity for some type of SO interaction which couples the spin and charge transport. For example, impurities with SO interaction will deflect spin-↑ (spin-↓) conduction electrons predominantly to the left (right) in the scattering process, thereby generating the *extrinsic* transverse spin Hall current. The theory of the extrinsic spin Hall effect has been around for several decades,[6–8] and it has recently been reexamined[11] to argue its major role in one of the two recent seminal experimental observations.[1] However, the extrinsic effect, which crucially relies on the presence of impurities with skew scattering and does not involve any SO coupling induced modification of the quasiparticle energy spectrum, is a rather small effect (unless one invokes band structure enhancement mechanisms involving intrinsic SO coupling in the bulk crystal which contributes a spin-dependent term to the impurity potential[11]) whose precise magnitude has been tantalizingly hard to estimate.[12]

Thus, a strong impetus for the revival of interest in the realm of the spin Hall effect has ascended from recent pre-

dictions for large pure spin currents flowing through (a) infinite homogeneous SO coupled semiconductors in the clean limit,[13,14] where the strong SO coupling induces the spin splitting of the quasiparticle energies, or (b) the electrodes of multiterminal finite-size mesoscopic nanostructures[15–17] made of such materials. However, the theory of the intrinsic spin Hall effect[18] in the bulk of infinite semiconductors is formulated in terms of the spin current density which is not conserved[3] in a medium with SO coupling and, therefore, does not have well-defined experimental measurement procedures associated with it. Moreover, these spin current densities can be nonzero even in thermodynamic equilibrium (with preserved time-reversal invariance).[19]

Theoretical scrutiny of such unusual features of the intrinsic spin Hall currents has led to major controversies:[18] (i) their dependence solely on the whole SO coupled Fermi sea and the spin-split band structure (e.g., the anomalous velocity due to the Berry curvature of Bloch states in *p*-doped semiconductors[13,20]), without any connection to nonequilibrium distribution function that characterizes conventional charge transport in the longitudinal direction,[21] have prompted arguments that such currents do not really transport spin or induce spin accumulation that would be useful for spintronics applications;[21,22] (ii) for the linear in momentum SO couplings, such as the Rashba or linear Dresselhaus coupling[4] in a two-dimensional electron gas (2DEG), numerous perturbative analytical[23–25] and nonperturbative numerical exact-diagonalization[26] studies find that the bulk intrinsic spin Hall current density (averaged over an infinite system[27]) vanishes for arbitrary small disorder, while being able to survive as edge spin current near the sample-electrode interfaces.[28,29] Also, the conclusions on the effect of different types of disorder (short-range versus long-range) are ambiguous[30] since they depend on the particular definition of the spin current density (conserved versus nonconserved[31]) employed in the calculation of the spin Hall conductivity defined for an infinite SO coupled system.

On the other hand, the mesoscopic spin Hall currents, predicted to flow out of ballistic phase-coherent samples made of various[15–17,32–34] SO coupled semiconductor systems through the attached transverse ideal (i.e., free of spin and charge interactions) leads, are conserved throughout the leads, depend only on the wave functions (or Green functions) at the Fermi surface (at low temperatures $T \to 0$), and are resilient to rather large static disorder $\Delta_{\mathrm{SO}}\tau/\hbar \gtrsim 10^{-1}$ (Δ_{SO} is the Rashba spin-splitting energy and τ is the elastic mean free time) within the diffusive metallic regime.[15,17] However, the theory of the *mesoscopic* spin Hall effect is formulated in terms of the Landauer-Büttiker-type transmission formalism[35] for spin currents,[15,16,36] which connects asymptotic scattering states in the leads without requiring any information about the quantum-mechanical probabilities for spin and charge propagation between two points inside the SO coupled sample. Technically, to obtain the spin Hall current flowing through the leads of a multiterminal device, one only needs the spin-dependent retarded real-space Green function connecting the sites residing in different leads, so that no information about its values between the points within the sample is required.[15]

Thus, many recent debates on the very existence of the spin Hall effect in clean SO coupled semiconductor structures could be resolved by visualizing the spatial details of the spin flow through experimentally accessible Hall bridges—from the SO coupled sample toward to attached electrodes with no SO interactions. Analogous studies of the spatial distribution of charge flow were essential in understanding the nature of quantum Hall transport (bulk versus edge[37]) in mesoscopic Hall bridges.[38,39] Furthermore, recent advances in multifarious scanning probe experimental techniques have made it possible to go beyond conventional transport measurements of macroscopically averaged quantities and image phase-coherent charge flow through a single 2DEG in the quantum Hall or quantum point-contact regime where the host semiconductor heterostructures is subjected to high or zero external magnetic field, respectively.[40] Comparable microscopic insights into the transport of spin have recently become available through advances in optical Kerr rotation microscopy for imaging of flowing spin densities.[41]

In particular, the theory of the imaging of charge flow can be obtained efficiently within the framework of lattice models of mesoscopic devices and the corresponding bond charge currents[35,42] which yield a detailed picture of the charge propagation between two arbitrary sites of the lattice.[43–45] Here we provide a tool that makes it possible to obtain the spatial details of the spin flow on the scale of a few nanometers by introducing *bond spin currents*, which represent the analog of bond charge currents as well as a lattice version of the spin current density[3] conventionally employed in studies of the intrinsic spin Hall effect in macroscopic systems.[13,14,23,24,28]

As shown in Sec. II, the bond spin currents can be computed efficiently in terms of the spin-resolved Keldysh Green functions[46] applied to the Landauer setup where a finite-size SO coupled semiconductor sample is attached to many semi-infinite ideal leads.[43,44,47] They are evaluated in Sec. III for a paradigmatic mesoscopic spin Hall generator—a four-terminal ballistic 2DEG with the Rashba type of SO coupling—to show the spatial profiles of spin currents and steady-state spin densities, thereby revealing features of the spin Hall transport on the nanoscale. In Sec. IV we show that local spin currents remain nonzero throughout the whole 2DEG even in the diffusive transport regime, in contrast to conjectures[28] put forth for macroscopic 2DEG's attached to massive electrodes where only the edge spin currents can survive disorder effects in Rashba spin-split systems. The integration of the linear response bond spin currents over the transverse cross sections allows us to connect in Sec. V the spin transport within the sample to the total spin Hall currents, which are obtained from the Landauer-Büttiker multiprobe spin current formulas,[15] flowing in an out of the 2DEG through the leads as a response to the applied voltages at the device boundaries. We conclude in Sec. VI.

II. BOND SPIN CURRENTS IN MULTITERMINAL NANOSTRUCTURES: LANDAUER-KELDYSH APPROACH

The conservation of charge implies the continuity equation in quantum mechanics for the charge density $\rho = e|\Psi(\mathbf{r})|^2$ associated with a given wave function $\Psi(\mathbf{r})$,

$$\frac{\partial \rho}{\partial t} + \boldsymbol{\nabla} \cdot \mathbf{j} = 0, \tag{1}$$

from which one can extract the expression for the charge current density:

$$\mathbf{j} = e\,\mathrm{Re}[\Psi^\dagger(\mathbf{r})\hat{\mathbf{v}}\Psi(\mathbf{r})]. \tag{2}$$

This can be viewed as the quantum-mechanical expectation value [in the state $\Psi(\mathbf{r})$] of the charge current density operator

$$\hat{\mathbf{j}} = e\frac{\hat{n}(\mathbf{r})\hat{\mathbf{v}} + \hat{\mathbf{v}}\hat{n}(\mathbf{r})}{2}. \tag{3}$$

Such operator can also be obtained heuristically from the classical charge current density $\mathbf{j}=en(\mathbf{r})\mathbf{v}$ via a quantization procedure where the particle density $n(\mathbf{r})$ and the velocity $\mathbf{v}$ are replaced by the corresponding operators and symmetrized to ensure that $\hat{\mathbf{j}}$ is a Hermitian operator.[35]

In SO coupled systems $\hat{\mathbf{j}}$ acquires extra terms since the velocity operator $i\hbar\hat{\mathbf{v}}=[\hat{\mathbf{r}},\hat{H}]$ is modified by the presence of SO terms in the Hamiltonian $\hat{H}$. For example, for the effective-mass Rashba Hamiltonian of a finite-size 2DEG (in the xy plane),

$$\hat{H} = \frac{\hat{\mathbf{p}}^2}{2m^*} + \frac{\alpha}{\hbar}(\hat{p}_y\hat{\sigma}_x - \hat{p}_x\hat{\sigma}_y) + V_{\mathrm{conf}}(x,y), \tag{4}$$

the velocity operator is

$$\hat{\mathbf{v}} = \frac{\hat{\mathbf{p}}}{m^*} - \frac{\alpha}{\hbar}(\hat{\sigma}_y\mathbf{e}_x - \hat{\sigma}_x\mathbf{e}_y), \tag{5}$$

where $\mathbf{e}_x$ and $\mathbf{e}_y$ are the unit vectors along the x and y axes, respectively. Here $\hat{\mathbf{p}}=(\hat{p}_x,\hat{p}_y)$ is the momentum operator in 2D, $\hat{\boldsymbol{\sigma}}=(\hat{\sigma}_x,\hat{\sigma}_y,\hat{\sigma}_z)$ is the vector of the Pauli spin matrices, α is the strength of the Rashba SO coupling[3,4] arising due to the structure inversion asymmetry,[48] and $V_{\mathrm{conf}}(x,y)$ is the transverse confining potential.

In contrast to the charge continuity equation (1), the analogous continuity equation for the spin density $S^i=(\hbar/2)\times[\Psi^\dagger(\mathbf{r})\hat{\sigma}_i\Psi(\mathbf{r})]$,

$$\frac{\partial S^i}{\partial t} + \boldsymbol{\nabla} \cdot \boldsymbol{\mathcal{J}}^i = F_s^i, \tag{6}$$

contains the spin current density

$$\boldsymbol{\mathcal{J}}^i = \frac{\hbar}{2}\Psi^\dagger(\mathbf{r})\frac{\hat{\sigma}_i\hat{\mathbf{v}} + \hat{\mathbf{v}}\hat{\sigma}_i}{2}\Psi(\mathbf{r}), \tag{7}$$

as well as a nonzero spin source term[49]

$$F_s^i = \frac{\hbar}{2}\,\mathrm{Re}\left(\Psi^\dagger(\mathbf{r})\frac{i}{\hbar}[\hat{H},\hat{\sigma}_i]\Psi(\mathbf{r})\right). \tag{8}$$

The nonzero $F_s^i \neq 0$ term reflects nonconservation of spin in the presence of SO couplings. Thus, the plausible Hermitian operator of the spin current density,[3]

$$\hat{\mathcal{J}}_k^i = \frac{\hbar}{2}\frac{\hat{\sigma}_i\hat{v}_k + \hat{v}_k\hat{\sigma}_i}{2}, \tag{9}$$

is a well-defined quantity (a tensor with nine components) only when the velocity operator is spin independent, as encountered in many metal spintronic devices.[50] Such a lack of physical justification for Eq. (9) in SO coupled systems leads to an arbitrariness[13] in the definition of the spin current density employed in recent intrinsic spin Hall studies,[31] thereby casting doubt on the experimental relevance of the quantitative predictions[13,14] for the spin Hall conductivity $\sigma_{sH}=\mathcal{J}_y^z/E_x$ computed as the linear response to the applied longitudinal electric field E_x penetrating an infinite SO coupled (perfect) semiconductor crystal.

To obtain the spatial profiles of spin and charge current densities in finite-size samples of arbitrary shape attached to many probes, it is advantageous to represent the spin-dependent Hamiltonian and the corresponding charge and spin current density operators in the local orbital basis.[42–44,47] For example, in such a representation the Rashba Hamiltonian can be recast in the form[9]

$$\hat{H} = \sum_{\mathbf{m}\sigma} \varepsilon_{\mathbf{m}}\hat{c}^\dagger_{\mathbf{m}\sigma}\hat{c}_{\mathbf{m}\sigma} + \sum_{\mathbf{m}\mathbf{m}'\sigma\sigma'} \hat{c}^\dagger_{\mathbf{m}\sigma}t^{\sigma\sigma'}_{\mathbf{m}\mathbf{m}'}\hat{c}_{\mathbf{m}'\sigma'}, \tag{10}$$

where the hard-wall boundary conditions account for confinement on the lattice $L_x\times L_y$ with the lattice spacing a. Here $\hat{c}^\dagger_{\mathbf{m}\sigma}$ ($\hat{c}_{\mathbf{m}\sigma}$) is the creation (annihilation) operator of an electron at the site $\mathbf{m}=(m_x,m_y)$.

While this Hamiltonian is of tight-binding type, its hopping parameters are nontrivial 2×2 Hermitian matrices $\mathbf{t}_{\mathbf{m}'\mathbf{m}}=(\mathbf{t}_{\mathbf{m}\mathbf{m}'})^\dagger$ in the spin space. The on-site potential $\varepsilon_{\mathbf{m}}$ describes any static local potential, such as the electrostatic potential due to the applied voltage or the disorder simulated via a uniform random variable $\varepsilon_{\mathbf{m}}\in[-W/2,W/2]$. The generalized nearest-neighbor hopping $t^{\sigma\sigma'}_{\mathbf{m}\mathbf{m}'}=(\mathbf{t}_{\mathbf{m}\mathbf{m}'})_{\sigma\sigma'}$ accounts for the Rashba coupling

$$\mathbf{t}_{\mathbf{m}\mathbf{m}'} = \begin{cases} -t_{\mathrm{o}}\mathbf{I}_s - it_{\mathrm{SO}}\hat{\sigma}_y & (\mathbf{m}=\mathbf{m}'+\mathbf{e}_x), \\ -t_{\mathrm{o}}\mathbf{I}_s + it_{\mathrm{SO}}\hat{\sigma}_x & (\mathbf{m}=\mathbf{m}'+\mathbf{e}_y), \end{cases} \tag{11}$$

through the SO hopping parameter $t_{\mathrm{SO}}=\alpha/2a$ ($\mathbf{I}_s$ is the unit 2×2 matrix in the spin space). A direct correspondence between the continuous effective Rashba Hamiltonian, Eq. (4) (with quadratic and isotropic energy-momentum dispersion), and its lattice version Eq. (10) (with tight-binding dispersion) is established by selecting the Fermi energy ($E_F=-3.8t_{\mathrm{o}}$ in the rest of the paper) of the injected electrons to be close to the bottom of the band $E_b=-4.0t_{\mathrm{o}}$ (so that tight-binding dispersion reduces to the quadratic one) and by using $t_{\mathrm{o}}=\hbar^2/(2m^*a^2)$ for the orbital hopping which yields the effective mass m^* in the continuum limit. For example, the InGaAs/InAlAs heterostructure employed in experiments of Ref. 51 is characterized by the effective mass $m^*=0.05m_0$ (m_0 is the free-electron mass) and the width of the conduction band $\Delta_b=0.9$ eV, which sets $t_{\mathrm{o}}=\Delta_b/8=112$ meV for the orbital hopping parameter on a square lattice (with four nearest neighbors of each site) and $a\simeq2.6$ nm for its lattice spacing. Thus, the Rashba SO coupling of 2DEG formed in this

heterostructure, tuned to a maximum value[51] $\alpha=0.93\times10^{-11}$ eV m by the gate voltage covering the 2DEG, corresponds to the SO hopping $t_{\mathrm{SO}}/t_{\mathrm{o}}\simeq0.016$ in the lattice Hamiltonian, Eq. (10).

The usage of the second-quantized notation in Eq. (10) facilitates the introduction of Keldysh Green-function[46] expressions for the nonequilibrium expectation values.[43,47] We imagine that at time $t'=-\infty$ the sample and leads are not connected, while the left and right longitudinal leads of a four-probe device are in their own thermal equilibrium with the chemical potentials μ_L and μ_R, respectively, where $\mu_L=\mu_R+eV$. The adiabatic switching of the hopping parameter connecting the leads and sample generates a time evolution of the density matrix of the structure.[47] The physical quantities are obtained as the nonequilibrium statistical average $\langle\cdots\rangle$ (with respect to the density matrix[46] at time $t'=0$) of the corresponding quantum-mechanical operators expressed in terms of $\hat{c}^{\dagger}_{\mathbf{m}\sigma}$ and $\hat{c}_{\mathbf{m}\sigma}$. This will lead to the expressions of the type $\langle\hat{c}^{\dagger}_{\mathbf{m}\sigma}\hat{c}_{\mathbf{m}\sigma'}\rangle$, which introduce the lesser Green function[43,47]

$$\langle\hat{c}^{\dagger}_{\mathbf{m}\sigma}\hat{c}_{\mathbf{m}'\sigma'}\rangle=\frac{\hbar}{i}G^{<}_{\mathbf{m}'\mathbf{m},\sigma'\sigma}(\tau=0)=\frac{1}{2\pi i}\int_{-\infty}^{\infty}dEG^{<}_{\mathbf{m}'\mathbf{m},\sigma'\sigma}(E). \tag{12}$$

Here we utilize the fact that the two-time correlation function $[\hat{c}_{\mathbf{m}\sigma}(t)=e^{i\hat{H}t/\hbar}\hat{c}_{\mathbf{m}\sigma}e^{-i\hat{H}t/\hbar}]$

$$G^{<}_{\mathbf{m}\mathbf{m}',\sigma\sigma'}(t,t')\equiv\frac{i}{\hbar}\langle\hat{c}^{\dagger}_{\mathbf{m}'\sigma'}(t')\hat{c}_{\mathbf{m}\sigma}(t)\rangle \tag{13}$$

depends only on $\tau=t-t'$ in stationary situations, so the time difference τ can be Fourier transformed to energy

$$G^{<}_{\mathbf{m}\mathbf{m}',\sigma\sigma'}(\tau)=\frac{1}{2\pi\hbar}\int_{-\infty}^{\infty}dEG^{<}_{\mathbf{m}\mathbf{m}',\sigma\sigma'}(E)e^{iE\tau/\hbar}, \tag{14}$$

which will be utilized for steady-state transport studied here. We use the notation where $\mathbf{G}^{<}_{\mathbf{m}\mathbf{m}'}$ is a 2×2 matrix in the spin space whose $\sigma\sigma'$ element is $G^{<}_{\mathbf{m}\mathbf{m}',\sigma\sigma'}$.

A. Bond charge currents in SO coupled systems

1. Bond charge-current operator

The charge conservation expressed through the familiar continuity equation (1) yields a uniquely determined bond charge-current operator for quantum systems described on a lattice by a tight-binding-type of Hamiltonian, Eq. (10). That is, the Heisenberg equation of motion

$$\frac{d\hat{N}_{\mathbf{m}}}{dt}=\frac{1}{i\hbar}[\hat{N}_{\mathbf{m}},\hat{H}], \tag{15}$$

for the electron number operator $\hat{N}_{\mathbf{m}}$ on site $\mathbf{m}$,

$$\hat{N}_{\mathbf{m}}\equiv\sum_{\sigma=\uparrow,\downarrow}\hat{c}^{\dagger}_{\mathbf{m}\sigma}\hat{c}_{\mathbf{m}\sigma}, \tag{16}$$

leads to the charge continuity equation on the lattice:

$$e\frac{d\hat{N}_{\mathbf{m}}}{dt}+\sum_{k=x,y}(\hat{J}_{\mathbf{m},\mathbf{m}+\mathbf{e}_k}-\hat{J}_{\mathbf{m}-\mathbf{e}_k,\mathbf{m}})=0. \tag{17}$$

This equation introduces the bond charge-current operator[35,42] $\hat{J}_{\mathbf{m}\mathbf{m}'}$ which describes the particle current from site $\mathbf{m}$ to its nearest neighbor site $\mathbf{m}'$ (the "bond" terminology is supported by a picture where current between two sites is represented by a bundle of flow lines bunched together along a line joining the two sites[42]).

Thus, the spin-dependent Hamiltonian, Eq. (10), containing 2×2 matrix hoppings defines the bond charge-current operator $\hat{J}_{\mathbf{m}\mathbf{m}'}=\Sigma_{\sigma\sigma'}\hat{J}^{\sigma\sigma'}_{\mathbf{m}\mathbf{m}'}$ which can be viewed as the sum of four different *spin-resolved* bond charge-current operators

$$\hat{J}^{\sigma\sigma'}_{\mathbf{m}\mathbf{m}'}=\frac{e}{i\hbar}[\hat{c}^{\dagger}_{\mathbf{m}'\sigma'}t^{\sigma'\sigma}_{\mathbf{m}'\mathbf{m}}\hat{c}_{\mathbf{m}\sigma}-\mathrm{H.c.}], \tag{18}$$

where H.c. stands for the Hermitian conjugate of the first term. In particular, for the case of $t^{\sigma\sigma'}_{\mathbf{m}\mathbf{m}'}$ being determined by the Rashba SO interaction, Eq. (11), we can decompose the bond charge-current operator into two terms

$$\hat{J}_{\mathbf{m}\mathbf{m}'}=\hat{J}^{\mathrm{kin}}_{\mathbf{m}\mathbf{m}'}+\hat{J}^{\mathrm{SO}}_{\mathbf{m}\mathbf{m}'}, \tag{19}$$

which have transparent physical interpretation. The first term

$$\hat{J}^{\mathrm{kin}}_{\mathbf{m}\mathbf{m}'}=\frac{eit_{\mathrm{o}}}{\hbar}\sum_{\sigma}[\hat{c}^{\dagger}_{\mathbf{m}'\sigma}\hat{c}_{\mathbf{m}\sigma}-\mathrm{H.c.}] \tag{20}$$

can be denoted as "kinetic" since it originates only from the kinetic energy t_{o} and does not depend on the SO coupling energy t_{SO}. On the other hand, the second term

$$\hat{J}^{\mathrm{SO}}_{\mathbf{m}\mathbf{m}'}=\begin{cases}-\dfrac{4et_{\mathrm{SO}}}{\hbar^2}\hat{S}^{y}_{\mathbf{m}\mathbf{m}'} & (\mathbf{m}=\mathbf{m}'+\mathbf{e}_x),\\ +\dfrac{4et_{\mathrm{SO}}}{\hbar^2}\hat{S}^{x}_{\mathbf{m}\mathbf{m}'} & (\mathbf{m}=\mathbf{m}'+\mathbf{e}_y),\end{cases}$$
$$=+\frac{4et_{\mathrm{SO}}}{\hbar^2}((\mathbf{m}'-\mathbf{m})\times\hat{\mathbf{S}}_{\mathbf{m}\mathbf{m}'})_z \tag{21}$$

represents an additional contribution to the intersite charge current flow due to nonzero Rashba SO hopping t_{SO}. Here we also introduce the "bond spin-density" operator

$$\hat{\mathbf{S}}_{\mathbf{m}\mathbf{m}'}=\frac{\hbar}{4}\sum_{\alpha\beta}[\hat{c}^{\dagger}_{\mathbf{m}'\alpha}\hat{\boldsymbol{\sigma}}_{\alpha\beta}\hat{c}_{\mathbf{m}\beta}+\mathrm{H.c.}], \tag{22}$$

defined for the bond connecting the sites $\mathbf{m}$ and $\mathbf{m}'$, which reduces to the usual definition of the local spin-density operator for $\mathbf{m}=\mathbf{m}'$ [see Eq. (34)].

2. Nonequilibrium bond charge current

The formalism of bond charge current makes it possible to compute physically measurable[40] spatial profiles of local charge current density within the sample as the quantum-statistical average $\langle\cdots\rangle$ (with respect to a density matrix that has evolved over sufficiently long time so that nonequilibrium state and all relevant interactions are fully established)

of the bond charge-current operator in the nonequilibrium state,[43,44,47]

$$\langle \hat{J}_{\mathbf{mm}'} \rangle = \sum_{\sigma\sigma'} \langle \hat{J}^{\sigma\sigma'}_{\mathbf{mm}'} \rangle, \tag{23}$$

$$\langle \hat{J}^{\sigma\sigma'}_{\mathbf{mm}'} \rangle = \frac{-e}{\hbar} \int_{-\infty}^{\infty} \frac{dE}{2\pi} [t^{\sigma'\sigma}_{\mathbf{m}'\mathbf{m}} G^{<}_{\mathbf{mm}',\sigma\sigma'}(E) - t^{\sigma\sigma'}_{\mathbf{mm}'} G^{<}_{\mathbf{m}'\mathbf{m},\sigma'\sigma}(E)], \tag{24}$$

where we utilize Eq. (12) to express the local charge current in terms of the nonequilibrium lesser Green function. The spin-resolved bond charge current in Eq. (24) describes the flow of charges which start as spin-σ electrons at site $\mathbf{m}$ and end up as spin-σ' electrons at site $\mathbf{m}'$ where possible spin flips $\sigma \neq \sigma'$ (instantaneous or due to precession) are caused by spin-dependent interactions. The decomposition of the bond charge-current operator into kinetic and SO terms in Eq. (19) leads to a Green-function expression for the corresponding nonequilibrium bond charge currents $\langle \hat{J}_{\mathbf{mm}'} \rangle = \langle \hat{J}^{\mathrm{kin}}_{\mathbf{mm}'} \rangle + \langle \hat{J}^{\mathrm{SO}}_{\mathbf{mm}'} \rangle$ with kinetic and SO terms given by

$$\langle \hat{J}^{\mathrm{kin}}_{\mathbf{mm}'} \rangle = \frac{et_{\mathrm{o}}}{\hbar} \int_{-\infty}^{\infty} \frac{dE}{2\pi} \mathrm{Tr}_s [\mathbf{G}^{<}_{\mathbf{mm}'}(E) - \mathbf{G}^{<}_{\mathbf{m}'\mathbf{m}}(E)], \tag{25}$$

$$\langle \hat{J}^{\mathrm{SO}}_{\mathbf{mm}'} \rangle = \frac{et_{\mathrm{SO}}}{\hbar} \int_{-\infty}^{\infty} \frac{dE}{2\pi i} \mathrm{Tr}_s \{ [(\mathbf{m}' - \mathbf{m}) \times \hat{\boldsymbol{\sigma}}]_z \times [\mathbf{G}^{<}_{\mathbf{mm}'}(E) + \mathbf{G}^{<}_{\mathbf{m}'\mathbf{m}}(E)] \}. \tag{26}$$

Note, however, that the "kinetic" term is also influenced by the SO coupling through $\mathbf{G}^{<}$. In the absence of the SO coupling, Eq. (26) vanishes and the bond charge current reduces to the standard expression.[43,44,47] The trace Tr_s here is performed in the spin Hilbert space. Similarly, we can also obtain the nonequilibrium local charge density in terms of $\mathbf{G}^{<}$,

$$e\langle \hat{N}_{\mathbf{m}} \rangle = e \sum_{\sigma=\uparrow,\downarrow} \langle \hat{c}^{\dagger}_{\mathbf{m}\sigma} \hat{c}_{\mathbf{m}\sigma} \rangle = \frac{e}{2\pi i} \int_{-\infty}^{\infty} dE \sum_{\sigma} G^{<}_{\mathbf{mm},\sigma\sigma}(E) = \frac{e}{2\pi i} \int_{-\infty}^{\infty} dE \mathrm{Tr}_s [\mathbf{G}^{<}_{\mathbf{mm}}(E)], \tag{27}$$

which is the statistical average value of the corresponding operator, Eq. (16).

B. Bond spin currents in SO coupled systems

1. Bond spin-current operator

To mimic the plausible definition of the spin-current density operator $\hat{\mathcal{J}}^i_k$ in Eq. (9), we can introduce the bond spin-current operator for the spin-S_i component as the symmetrized product of the spin-$\frac{1}{2}$ operator $\hbar\hat{\sigma}_i/2$ $(i=x,y,z)$ and the bond charge-current operator from Eq. (17):

$$\hat{J}^{S_i}_{\mathbf{mm}'} \equiv \frac{1}{4i} \sum_{\alpha\beta} [\hat{c}^{\dagger}_{\mathbf{m}'\beta} \{\hat{\sigma}_i, \mathbf{t}_{\mathbf{m}'\mathbf{m}}\}_{\beta\alpha} \hat{c}_{\mathbf{m}\alpha} - \mathrm{H.c.}]. \tag{28}$$

By inserting the hopping matrix $\mathbf{t}_{\mathbf{m}'\mathbf{m}}$, Eq. (11), of the lattice SO Hamiltonian into this expression we obtain its explicit expression for the Rashba SO coupled system:

$$\hat{J}^{S_i}_{\mathbf{mm}'} = \frac{it_{\mathrm{o}}}{2} \sum_{\alpha\beta} (\hat{c}^{\dagger}_{\mathbf{m}'\beta} (\hat{\sigma}_i)_{\beta\alpha} \hat{c}_{\mathbf{m}\alpha} - \mathrm{H.c.}) + t_{\mathrm{SO}} \hat{N}_{\mathbf{mm}'} [\mathbf{e}_i \times (\mathbf{m}' - \mathbf{m})]_z, \tag{29}$$

which can be considered as the lattice version of Eq. (9). Here we simplify the notation by using the "bond electron-number operator" $\hat{N}_{\mathbf{mm}'}$,

$$\hat{N}_{\mathbf{mm}'} \equiv \frac{1}{2} \sum_{\sigma} (\hat{c}^{\dagger}_{\mathbf{m}'\sigma} \hat{c}_{\mathbf{m}\sigma} + \mathrm{H.c.}), \tag{30}$$

which reduces to the standard electron-number operator, Eq. (16), for $\mathbf{m}=\mathbf{m}'$.

2. Nonequilibrium bond spin current

Similarly to the case of the nonequilibrium bond charge current in Sec. II A 2, the nonequilibrium statistical average of the bond-spin-current operator, Eq. (29), can be expressed using the lesser Green function $\mathbf{G}^{<}$ as

$$\langle \hat{J}^{S_i}_{\mathbf{mm}'} \rangle = \langle \hat{J}^{S_i(\mathrm{kin})}_{\mathbf{mm}'} \rangle + \langle \hat{J}^{S_i(\mathrm{so})}_{\mathbf{mm}'} \rangle, \tag{31}$$

$$\langle \hat{J}^{S_i(\mathrm{kin})}_{\mathbf{mm}'} \rangle = \frac{t_{\mathrm{o}}}{2} \int_{-\infty}^{\infty} \frac{dE}{2\pi} \mathrm{Tr}_s [\hat{\sigma}_i (\mathbf{G}^{<}_{\mathbf{m}'\mathbf{m}}(E) - \mathbf{G}^{<}_{\mathbf{mm}'}(E))], \tag{32}$$

$$\langle \hat{J}^{S_i(\mathrm{SO})}_{\mathbf{mm}'} \rangle = [\mathbf{e}_i \times (\mathbf{m}' - \mathbf{m})]_z \frac{t_{\mathrm{SO}}}{2} \int_{-\infty}^{\infty} \frac{dE}{2\pi i} \times \mathrm{Tr}_s [\mathbf{G}^{<}_{\mathbf{mm}'}(E) + \mathbf{G}^{<}_{\mathbf{m}'\mathbf{m}}(E)]. \tag{33}$$

Here we also encounter two terms which can be interpreted as the kinetic and SO contributions to the bond spin current crossing from site $\mathbf{m}$ to site $\mathbf{m}'$. However, we emphasize that such a SO contribution to the spin-S_z bond current is identically equal to zero, which simplifies the expression for this component to Eq. (32) studied in the rest of the paper as the primary spin current response in the spin Hall effect.

3. Local spin density and its continuity equation

The local spin density in the lattice models is determined by the local spin operator $\hat{\mathbf{S}}_{\mathbf{m}} = (\hat{S}^x_{\mathbf{m}}, \hat{S}^y_{\mathbf{m}}, \hat{S}^z_{\mathbf{m}})$ at site $\mathbf{m}$ defined by

$$\hat{\mathbf{S}}_{\mathbf{m}} = \frac{\hbar}{2} \sum_{\alpha\beta} \hat{c}^{\dagger}_{\mathbf{m}\alpha} \hat{\boldsymbol{\sigma}}_{\alpha\beta} \hat{c}_{\mathbf{m}\beta}. \tag{34}$$

The Heisenberg equation of motion for each component $\hat{\mathbf{S}}_i$ $(i=x,y,z)$ of the spin density operator

$$\frac{d\hat{S}^i_{\mathbf{m}}}{dt} = \frac{1}{i\hbar}[\hat{S}^i_{\mathbf{m}}, \hat{H}] \tag{35}$$

can be written in the form

$$\frac{d\hat{S}^i_{\mathbf{m}}}{dt} + \sum_{k=x,y} (\hat{J}^{S_i}_{\mathbf{m},\mathbf{m}+\mathbf{e}_k} - \hat{J}^{S_i}_{\mathbf{m}-\mathbf{e}_k,\mathbf{m}}) = \hat{F}^{S_i}_{\mathbf{m}}, \tag{36}$$

where $\hat{J}^{S_i}_{\mathbf{mm}'}$ is the bond spin-current operator given by Eq. (28) so that the second term on the left-hand side of Eq. (36) corresponds to the "divergence" of the bond spin current on site $\mathbf{m}$. Here, in analogy with Eq. (8), we also find the lattice version of the spin source operator $\hat{F}^{S_i}_{\mathbf{m}}$ whose explicit form is

$$\hat{F}^{S_x}_{\mathbf{m}} = -\frac{t_{\mathrm{SO}}}{t_{\mathrm{o}}}(\hat{J}^{S_z}_{\mathbf{m},\mathbf{m}+\mathbf{e}_x} + \hat{J}^{S_z}_{\mathbf{m}-\mathbf{e}_x,\mathbf{m}}), \tag{37}$$

$$\hat{F}^{S_y}_{\mathbf{m}} = -\frac{t_{\mathrm{SO}}}{t_{\mathrm{o}}}(\hat{J}^{S_z}_{\mathbf{m},\mathbf{m}+\mathbf{e}_y} + \hat{J}^{S_z}_{\mathbf{m}-\mathbf{e}_y,\mathbf{m}}), \tag{38}$$

$$\hat{F}^{S_z}_{\mathbf{m}} = \frac{t_{\mathrm{SO}}}{t_{\mathrm{o}}}(\hat{J}^{S_x}_{\mathbf{m},\mathbf{m}+\mathbf{e}_x} + \hat{J}^{S_x}_{\mathbf{m}-\mathbf{e}_x,\mathbf{m}} + \hat{J}^{S_y}_{\mathbf{m},\mathbf{m}+\mathbf{e}_y} + \hat{J}^{S_y}_{\mathbf{m}-\mathbf{e}_y,\mathbf{m}}). \tag{39}$$

The presence of the nonzero term $\hat{F}^{S_i}_{\mathbf{m}}$ on the right-hand side of the spin continuity equation (36) signifies, within the framework of bond spin-current formalism, the fact that spin is not conserved in SO coupled systems where it is forced into precession by the effective momentum-dependent magnetic field corresponding to the SO coupling. The fact that the bond spin-current operator, Eq. (28), appears in the spin continuity equation (36) as its divergence implies that its definition in Eq. (28) is plausible. However, the presence of the spin source operator $\hat{F}^{S_i}_{\mathbf{m}}$ reminds us that such a definition cannot be made unique,[31] unlike the case of the bond charge current which is uniquely determined by the charge continuity equation (17).

If we evaluate the statistical average of Eq. (36) in a steady state (which can be either equilibrium or nonequilibrium), we obtain the identity

$$\sum_{k=x,y} (\langle \hat{J}^{S_i}_{\mathbf{m},\mathbf{m}+\mathbf{e}_k} \rangle - \langle \hat{J}^{S_i}_{\mathbf{m}-\mathbf{e}_k,\mathbf{m}} \rangle) = \langle \hat{F}^{S_i}_{\mathbf{m}} \rangle. \tag{40}$$

In particular, for the spin-S_z component we get

$$\sum_{k=x,y} (\langle \hat{J}^{S_z}_{\mathbf{m},\mathbf{m}+\mathbf{e}_k} \rangle - \langle \hat{J}^{S_z}_{\mathbf{m}-\mathbf{e}_k,\mathbf{m}} \rangle) = \frac{t_{\mathrm{SO}}}{t_{\mathrm{o}}} \sum_{k=x,y} (\langle \hat{J}^{S_k}_{\mathbf{m},\mathbf{m}+\mathbf{e}_k} \rangle + \langle \hat{J}^{S_k}_{\mathbf{m}-\mathbf{e}_k,\mathbf{m}} \rangle), \tag{41}$$

which relates the divergence of the spin-S_z current (left-hand side) to the spin source (right-hand side) determined by the sum of the longitudinal component of the spin-S_x current and the transverse component of the spin-S_y current.

Since no experiment has been proposed to measure local spin current density within the SO coupled sample, defined through Eq. (7) or its lattice equivalent, Eq. (31), we can obtain additional information about the spin fluxes within the sample by computing the local spin density

$$\begin{aligned}\langle \hat{\mathbf{S}}_{\mathbf{m}} \rangle &= \frac{\hbar}{2} \sum_{\alpha,\beta=\uparrow,\downarrow} \hat{\boldsymbol{\sigma}}_{\alpha\beta} \langle \hat{c}^\dagger_{\mathbf{m}\alpha} \hat{c}_{\mathbf{m}\beta} \rangle \\ &= \frac{\hbar}{4\pi i} \int_{-\infty}^{\infty} dE \sum_{\alpha,\beta=\uparrow,\downarrow} \hat{\boldsymbol{\sigma}}_{\alpha\beta} G^<_{\mathbf{mm},\beta\alpha}(E) \\ &= \frac{\hbar}{4\pi i} \int_{-\infty}^{\infty} dE \mathrm{Tr}_s[\hat{\boldsymbol{\sigma}} \mathbf{G}^<_{\mathbf{mm}}(E)]. \end{aligned} \tag{42}$$

Motivated by recent advances in Kerr rotation microscopy, which have made possible experimental imaging of steady-state spin polarization in various SO coupled semiconductor structures,[41] we will also plot spatial profiles of $\langle \hat{\mathbf{S}}_{\mathbf{m}} \rangle$ as a well-defined and measurable quantity that offers insight into the spin flow in the nonequilibrium steady transport state.

C. Spin-resolved Landauer-Keldysh Green functions for finite-size mesoscopic devices

The formalism discussed thus far does not depend on the details of the external driving force which brings the system into a nonequilibrium state. That is, the system can be driven by either the homogeneous electric field applied to an infinite homogeneous 2DEG or the voltage (i.e., electrochemical potential) difference between the electrodes attached to a finite-size *mesoscopic* sample. For example, in the latter case, the external bias voltage only shifts the relative chemical potentials of the reservoirs into which the longitudinal leads (employed to simplify the boundary conditions) eventually terminate, so that the electrons do not feel any electric field in the course of ballistic propagation through clean 2DEG central region. The information about these different situations is encoded into the lesser Green function $\mathbf{G}^<$.

Here we focus on experimentally accessible spin Hall bridges[15] where the finite-size central region (C), defined on the $L \times L$ lattice, is attached to four external semi-infinite leads of the same width L. The leads at infinity terminate into the reservoirs where electrons are brought into thermal equilibrium, characterized by the Fermi-Dirac distribution function $f(E-eV_p)$, to ensure the steady-state transport. In such Landauer setup[35] current is limited by quantum transmission through a potential profile while power is dissipated nonlocally in the reservoirs. The voltage in each lead of the four-terminal spin Hall bridge is V_p ($p=1,\ldots,4$) so that the on-site potential $\varepsilon_{\mathbf{m}}$ within the leads has to be shifted by eV_p.

The spin-dependent lesser Green function $\mathbf{G}^<$ defined in Eq. (13) is evaluated within the finite-size sample region as a $2L^2 \times 2L^2$ matrix in the site$\otimes$spin space through the spin-resolved Keldysh equation for matrices,[9]

$$\mathbf{G}^<(E) = \mathbf{G}(E)\boldsymbol{\Sigma}^<(E)\mathbf{G}^\dagger(E), \tag{43}$$

which is valid in this form for steady-state transport when transients have died away.[46] Within the effective single-particle picture, the retarded Green function can be obtained by inverting the Hamiltonian

$$\mathbf{G}(E) = \left[E\mathbf{I}_C - \mathbf{H}_C - eU_{\mathbf{m}} - \sum_p \Sigma_p(E - eV_p) \right]^{-1}, \quad (44)$$

where the self-energies

$$\Sigma^<(E) = i\sum_p \Gamma_p(E - eV_p) f(E - eV_p), \quad (45)$$

$$\Gamma_p(E) = i[\Sigma_p(E) - \Sigma_p^\dagger(E)], \quad (46)$$

$$\Sigma_p(E) = \mathbf{H}_{pC}^\dagger [(E + i0_+)\mathbf{I}_p - \mathbf{H}_p^{\text{lead}}]^{-1} \mathbf{H}_{pC} \quad (47)$$

are exactly computable in the noninteracting electron approximation and without any inelastic processes taking place within the sample. They take into account the "interaction" of the SO coupled sample with the attached leads and generate a finite lifetime that an electron spends within the 2DEG before escaping through the leads toward the macroscopic thermalizing reservoirs. Here $\mathbf{I}_C$ is the $2L^2 \times 2L^2$ identity matrix and $\mathbf{I}_p$ is the identity matrix in the infinite site $\otimes$ spin space of the lead p. We use the Hamiltonian matrices

$$(\mathbf{H}_C)_{\mathbf{m}\mathbf{m}',\sigma\sigma'} = \langle 1_{\mathbf{m}\sigma} | \hat{H} | 1_{\mathbf{m}'\sigma'} \rangle \quad (\mathbf{m}, \mathbf{m}' \in C),$$

$$(\mathbf{H}_p^{\text{lead}})_{\mathbf{m}\mathbf{m}',\sigma\sigma'} = \langle 1_{\mathbf{m}\sigma} | \hat{H} | 1_{\mathbf{m}'\sigma'} \rangle \quad (\mathbf{m}, \mathbf{m}' \in p),$$

$$(\mathbf{H}_{pC})_{\mathbf{m}\mathbf{m}',\sigma\sigma'} = \langle 1_{\mathbf{m}\sigma} | \hat{H} | 1_{\mathbf{m}'\sigma'} \rangle \quad (\mathbf{m} \in p, \mathbf{m}' \in \mathrm{C}), \quad (48)$$

where $|1_{\mathbf{m}\sigma}\rangle$ is a vector in the Fock space (meaning that the occupation number is one for the single-particle state $|\mathbf{m}\sigma\rangle$ and zero otherwise) and $\hat{H}$ is the Hamiltonian given in Eq. (10).

In the general case of arbitrary applied bias voltage, the gauge invariance of measurable quantities (such as the current-voltage characteristic) with respect to the shift of electric potential everywhere by a constant V, $eV_p \to eV_p + eV$ and $eU_{\mathbf{m}} \to eU_{\mathbf{m}} + eV$, is satisfied on the proviso that the retarded self-energies $\Sigma_p(E - eV_p)$ introduced by each lead depend explicitly on the applied voltages at the sample boundary, while the computation of the retarded Green function $\mathbf{G}(E)$ has to include the electric potential landscape $U_{\mathbf{m}}$ within the sample[52] [which can be obtained from the Poisson equation with charge density, Eq. (27)]. However, when the applied bias is low, so that linear response zero-temperature quantum transport takes place through the sample [as determined by $\mathbf{G}(E_F)$], the exact profile of the internal potential becomes irrelevant.[35,53]

III. SPATIAL PROFILES OF LOCAL SPIN CURRENTS AND SPIN DENSITIES IN BALLISTIC FOUR-TERMINAL RASHBA SO COUPLED NANOSTRUCTURES

Under time-reversal transformation, the mass, charge, and energy do not change sign, while the velocity operator and the Pauli matrices change sign,[54] $t \to -t \Rightarrow \hat{\mathbf{v}} \to -\hat{\mathbf{v}}$ and $t \to -t \Rightarrow \hat{\sigma} \to -\hat{\sigma}$. Since the charge-current density operator, Eq. (3), contains velocity, it changes sign under the time reversal $t \to -t \Rightarrow \hat{\mathbf{j}} \to -\hat{\mathbf{j}}$ and, therefore, has to vanish in the thermodynamic equilibrium (except in the presence of an external magnetic field which breaks time-reversal invariance, thereby allowing for circulating or diamagnetic charge currents even in thermodynamic equilibrium[35,39]). On the other hand, the spin-current density operator, Eq. (9), which is the product of the velocity and Pauli matrices, is the time-reversal invariant quantity $t \to -t \Rightarrow \hat{\mathcal{J}}_k^i \to \hat{\mathcal{J}}_k^i$: if the clock ran backward, spin current would continue to flow in the same direction. Thus, $\hat{\mathcal{J}}_k^i$ can have nonzero expectation values even in thermodynamic equilibrium and in the absence of external magnetic fields. This has been explicitly demonstrated[19] for the case of an infinite clean Rashba spin-split 2DEG where such *equilibrium* spin currents are polarized inside the plane.[19] Thus, the out-of-plane polarized spin-current density in the bulk has been considered as a genuine nonequilibrium spin-Hall-effect-induced response.[14] However, no analysis of the properties of equilibrium spin currents in finite-size multiterminal devices with SO coupling has been undertaken—this is essential information for the development of a consistent theory for transport (nonequilibrium) spin currents where contributions from background (equilibrium) currents must be eliminated.[19]

To investigate microscopic profiles of equilibrium local spin currents in mesoscopic *finite-size* devices we plot in Fig. 1(a) the spatial distribution of the bond spin currents, carried by the whole Fermi sea, in a four-terminal ballistic device with no impurities where all leads are kept at the same potential V_p=const. Although we find nonzero local spin currents (for the S_z component of spin), they *do not* transport any spin since the *total* spin current, obtained by summing the bond spin currents over an arbitrary transverse cross section of the device

$$I_{\text{trans}}^{S_z}(m_y) = \sum_{m_x} \langle \hat{J}^{S_z}_{(m_x,m_y)(m_x,m_y+1)} \rangle \quad (49)$$

or over any longitudinal cross section

$$I_{\text{long}}^{S_z}(m_x) = \sum_{m_y} \langle \hat{J}^{S_z}_{(m_x,m_y)(m_x+1,m_y)} \rangle, \quad (50)$$

is identically equal to zero $I_{\text{trans}}^{S_z(\text{eq})}(m_y) = I_{\text{long}}^{S_z(\text{eq})}(m_x) \equiv 0$. Note that equilibrium currents in Fig. 1(a), whose spin is polarized orthogonal to the plane, emerge here because of the boundaries of the finite-size device—in infinite Rashba SO coupled 2DEG's such out-of-plane polarized equilibrium spin currents are found to be zero, $\mathcal{J}_x^z = \mathcal{J}_y^z \equiv 0$, while the in-plane polarized ones satisfy the relations[19] $\mathcal{J}_x^x = \mathcal{J}_y^y \equiv 0$ and $\mathcal{J}_y^x = -\mathcal{J}_x^y$.

To investigate manifestations of in-plane polarized equilibrium spin currents in finite-size multiterminal devices, we plot in Fig. 2 the spatial profiles of the corresponding equilibrium bond spin currents $\langle \hat{J}^{S_x(\text{eq})}_{\mathbf{m}\mathbf{m}'} \rangle$ and $\langle \hat{J}^{S_y(\text{eq})}_{\mathbf{m}\mathbf{m}'} \rangle$ obtained from Eq. (31) with V=0 and integration over the whole Fermi sea (i.e., from the band bottom to the Fermi energy E_F). While these spatial profiles do not satisfy the simple symmetry properties found by Rashba[19] in infinite 2DEG's,

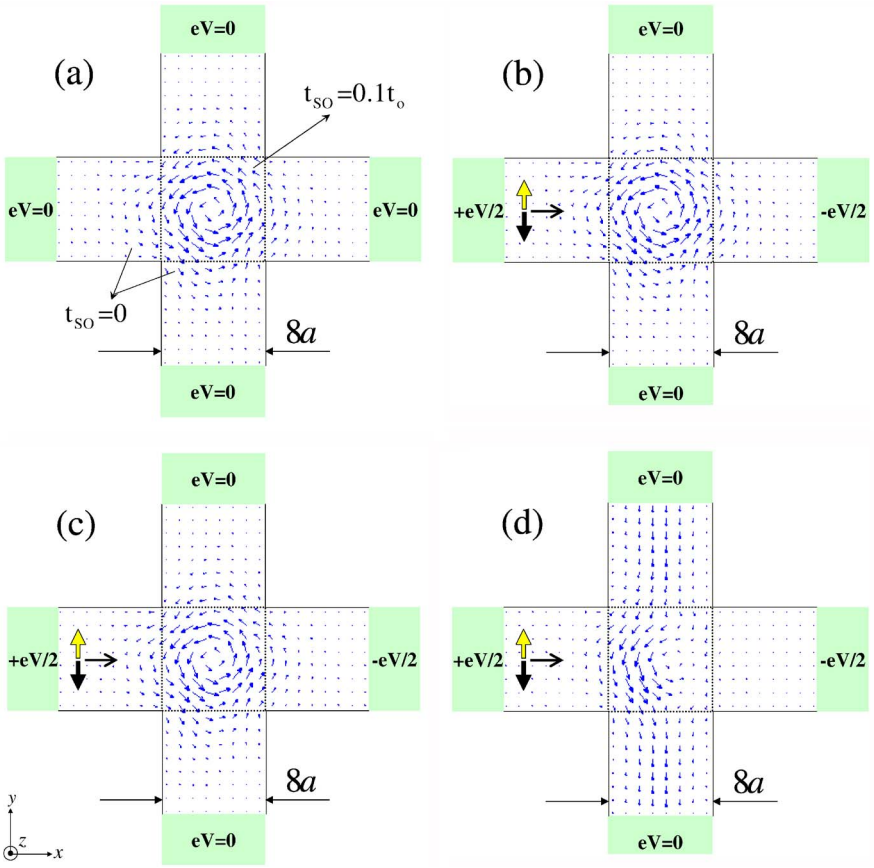

FIG. 1. (Color online) The spatial distribution of local spin currents in ballistic four-terminal bridges where the central 2DEG region, with the Rashba SO coupling $t_{\mathrm{SO}}=0.1t_{\mathrm{o}}$ and the corresponding spin precession length $L_{\mathrm{SO}}=\pi t_{\mathrm{o}}a/2t_{\mathrm{SO}}\approx 15.7a$ (typically $a\simeq 3$ nm), is attached to four ideal ($t_{\mathrm{SO}}\equiv 0$) leads. The magnitude of the bond spin current is proportional to the length of the arrow. The device is in equilibrium ($V_p=0$) in (a) and out of equilibrium in (b), (c), and (d) due to the applied bias voltage $eV=10^{-3}t_{\mathrm{o}}$ which drives the linear response longitudinal charge current and the transverse spin Hall current induced by its passage through the SO coupled region. The local spin current in (b), which is "carried" by all states from $-4t_{\mathrm{o}}$ (band bottom) to $E_F+eV/2$ ($E_F=-3.8t_{\mathrm{o}}$), is the sum of equilibrium (persistent) spin current $\langle\hat{J}^{S_z(\mathrm{eq})}_{\mathbf{mm'}}\rangle$ in (c), carried by the fully occupied states from $-4t_{\mathrm{o}}$ to $E_F-eV/2$, and the nonequilibrium (transport) spin current $\langle\hat{J}^{S_z(\mathrm{neq})}_{\mathbf{mm'}}\rangle$ in (d) carried by the partially occupied states around the Fermi energy from $\mu_R=E_F-eV/2$ (electrochemical potential of the right reservoir) to $\mu_L=E_F+eV/2$ (electrochemical potential of the left reservoir). Note that the sum of $\langle\hat{J}^{S_z(\mathrm{eq})}_{\mathbf{mm'}}\rangle$ in (c) over arbitrary transverse cross section (orthogonal to the y axis) gives zero total spin current through that cross section, while the same sum of $\langle\hat{J}^{S_z(\mathrm{neq})}_{\mathbf{mm'}}\rangle$ in (d) defines the total spin current which flows into the leads and is, in principle, experimentally measurable.

the total spin currents *within* the SO coupled region obey similar relations, $I^{S_x(\mathrm{eq})}_{\mathrm{trans}}(m_y)=-I^{S_y(\mathrm{eq})}_{\mathrm{long}}(m_x)$. We conclude the story of equilibrium spin currents in multiterminal nanostructures by stressing that microscopic picture offered by Figs. 1(a) and 2 yields direct visual proof of the fact that no equilibrium *total* spin currents, conjectured in Ref. 36, can actually appear in the leads of an unbiased ($V_p=$const) mesoscopic device in thermodynamic equilibrium, as demonstrated recently[16,55] within the Landauer-Büttiker approach (which operates only with measurable total charge and spin currents in the leads).

In Fig. 1(b) we apply low (i.e., linear response; see Sec. V) bias voltage $eV=10^{-3}t_{\mathrm{o}}\ll(E_F-E_b)=0.2t_{\mathrm{o}}$ between the longitudinal leads and integrate expression (32) from the bottom of the band to the chemical potential $E_F+eV/2$ of the left reservoir. In contrast to the equilibrium spin-current density from Fig. 1(a), the vortex pattern is now distorted and nonzero total spin current $I^{S_z}_{\mathrm{trans}}(m_y)\neq 0$ in Eq. (49) emerges in the transverse direction, as expected in the phenomenology of the spin Hall effect.

One of the highly unconventional features of the intrinsic spin Hall current density is its dependence on the whole SO coupled Fermi sea,[13,14] even when the infinite system is driven out of equilibrium by the applied external electric field, thereby limiting the charge transport (or the extrinsic spin Hall response) to the Fermi level through the nonequilibrium part of the distribution function.[21] However, such a property for physically relevant and experimentally measurable total currents (through some cross section) would be alien to the spirit of the Fermi-liquid theory where transport involves only quasiparticles whose energies are within k_BT of the Fermi level.

While the spin currents crossing the transverse bonds in Fig. 1(b) are apparently carried by the whole Fermi sea, we now separate the integration in Eq. (32) for S_z bond spin current into two parts:

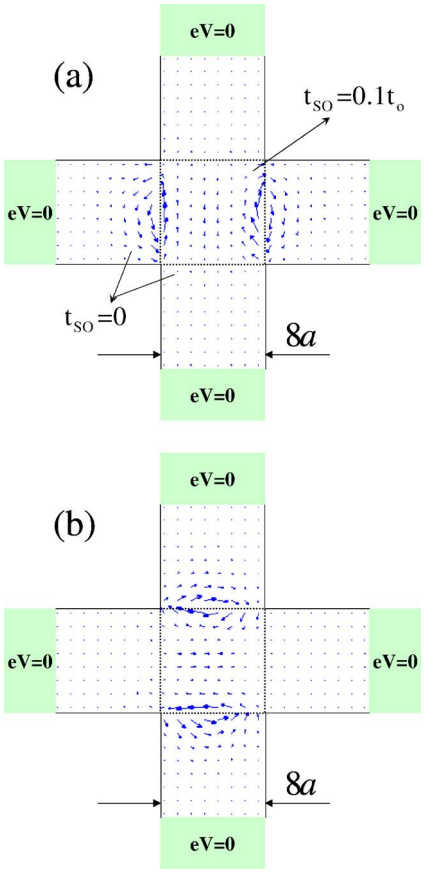

FIG. 2. (Color online) The spatial profiles of equilibrium local spin currents with in-plane spin polarization (a) $\langle \hat{J}^{S_x(\mathrm{eq})}_{\mathbf{mm}'} \rangle$ and (b) $\langle \hat{J}^{S_y(\mathrm{eq})}_{\mathbf{mm}'} \rangle$ in unbiased ($V_p=0$) ballistic four-terminal bridges where the central 2DEG region, with the Rashba SO coupling $t_{\mathrm{SO}}=0.1t_o$ and the corresponding spin precession length $L_{\mathrm{SO}}=\pi t_o a/2t_{\mathrm{SO}} \approx 15.7a$, is attached to four ideal ($t_{\mathrm{SO}}\equiv 0$) leads. These equilibrium bond spin currents are "carried" by the whole Fermi sea (i.e., they depend on all states from the band bottom at $-4t_o$ to the Fermi energy $E_F=-3.8t_o$).

$$\langle \hat{J}^{S_z}_{\mathbf{mm}'} \rangle = \frac{t_o}{2}\int_{E_b}^{E_F-eV/2} \frac{dE}{2\pi} \mathrm{Tr}_s\{\hat{\sigma}_z[\mathbf{G}^{<}_{\mathbf{m}'\mathbf{m}}(E) - \mathbf{G}^{<}_{\mathbf{mm}'}(E)]\} + \frac{t_o}{2}\int_{E_F-eV/2}^{E_F+eV/2} \frac{dE}{2\pi} \mathrm{Tr}_s\{\hat{\sigma}_z[\mathbf{G}^{<}_{\mathbf{m}'\mathbf{m}}(E) - \mathbf{G}^{<}_{\mathbf{mm}'}(E)]\} = \langle \hat{J}^{S_z(\mathrm{eq})}_{\mathbf{mm}'} \rangle + \langle \hat{J}^{S_z(\mathrm{neq})}_{\mathbf{mm}'} \rangle. \quad (51)$$

The states from the band bottom E_b to $E_F-eV/2$ are fully occupied, while states in the energy interval from the electrochemical potential $E_F-eV/2$ ($eV>0$) of the right reservoir to the electrochemical potential $E_F+eV/2$ of the left reservoir are partially occupied because of the competition between the left reservoir which tries to fill them and the right reservoir which tries to deplete them. The profile of the first term $\langle \hat{J}^{S_z(\mathrm{eq})}_{\mathbf{mm}'} \rangle$ in Eq. (51) is shown in Fig. 1(c), while the spatial profile of the second term, representing the local spin current $\langle \hat{J}^{S_z(\mathrm{neq})}_{\mathbf{mm}'} \rangle$ carried by the states around the Fermi energy, is shown in Fig. 1(d).

The spatial distribution of the microscopic spin currents in Fig. 1(c) is akin to the vortexlike pattern of bond spin currents within the device in equilibrium in Fig. 1(a) and, therefore, *does not* transport any spin between two points in real space. Thus, Fig. 1 convincingly demonstrates that nonzero-spin Hall flux through the transverse cross sections in Figs. 1(b) and 1(d) is due to only the wave functions (or Green functions) at the Fermi energy (as $T\to 0$), in accordance with the general paradigms of the Landau's Fermi-liquid theory where transport quantities are expected to be expressed as the Fermi-surface property.[35,56]

We recall here that a similar situation appears in charge transport in an external magnetic field where equilibrium (or persistent) current density,[35] or bond charge currents in the lattice formalism,[39,44] can be nonzero even in the unbiased devices in thermal equilibrium due to the breaking of time-reversal invariance by an external magnetic field. However, such circulating or diamagnetic currents carried by the Fermi sea, which in Landauer-Keldysh formalism can be subtracted by separating the integration[39] in a fashion similar to our Eq. (51), do not contribute to the net charge transport (i.e., to the total charge current measured in experiments) through any cross section of the device.[35,39] Thus, early "Fermi-sea" expressions for the linear response transport coefficients in, e.g., the quantum Hall effect theory[35] or in the anomalous Hall effect theory[56] were eventually recast in terms of the Fermi-surface-determined quantities. Similarly, Fig. 1 demonstrates that spin Hall current carried by the "bulk" of the Fermi sea, which is an equilibrium current and does not really transport spin between two points in space, should be subtracted[19] to obtain a theory for the intrinsic spin Hall conductivity that could be related to experimentally observable quantities.

One of the basic tests for theories of the spin Hall effect is to predict the direction of the spin Hall current or the corresponding sign[9,11,31] of nonequilibrium spin Hall accumulation deposited by such current on the lateral boundaries of experimental devices.[1,2] The nonequilibrium (linear response) spin Hall current in Fig. 1(d) flows from the top to the bottom transverse lead because the spin-$\uparrow$ electrons are deflected to the right. This feature can be understood using the semiclassical picture based on the SO force operator[57,58] generated by the Rashba Hamiltonian, Eq. (4), for the finite-size 2DEG:

$$\hat{\mathbf{F}}_{\mathrm{SO}} = \frac{2\alpha^2 m^*}{\hbar^3}(\hat{\mathbf{p}}\times\mathbf{z})\otimes\hat{\sigma}_z - \frac{dV_{\mathrm{conf}}(\hat{y})}{d\hat{y}}\mathbf{y}. \quad (52)$$

The apparently simple picture brought by the expectation values of Eq. (52) in the spin-polarized wave packet states $|\Psi\rangle\otimes|\uparrow\rangle$ also explains why the transverse spin Hall current density bends toward the right in Fig. 1 while passing through the SO coupled region.

However, this expectation value (i.e., the SO "force") oscillates along the sample due to the precession of the deflected spin in the effective Rashba magnetic field which is nearly parallel to the y axis because of transverse confinement effects.[57] In ballistic strongly coupled SO structures such an α^2-dependent SO "force," which oscillates on the

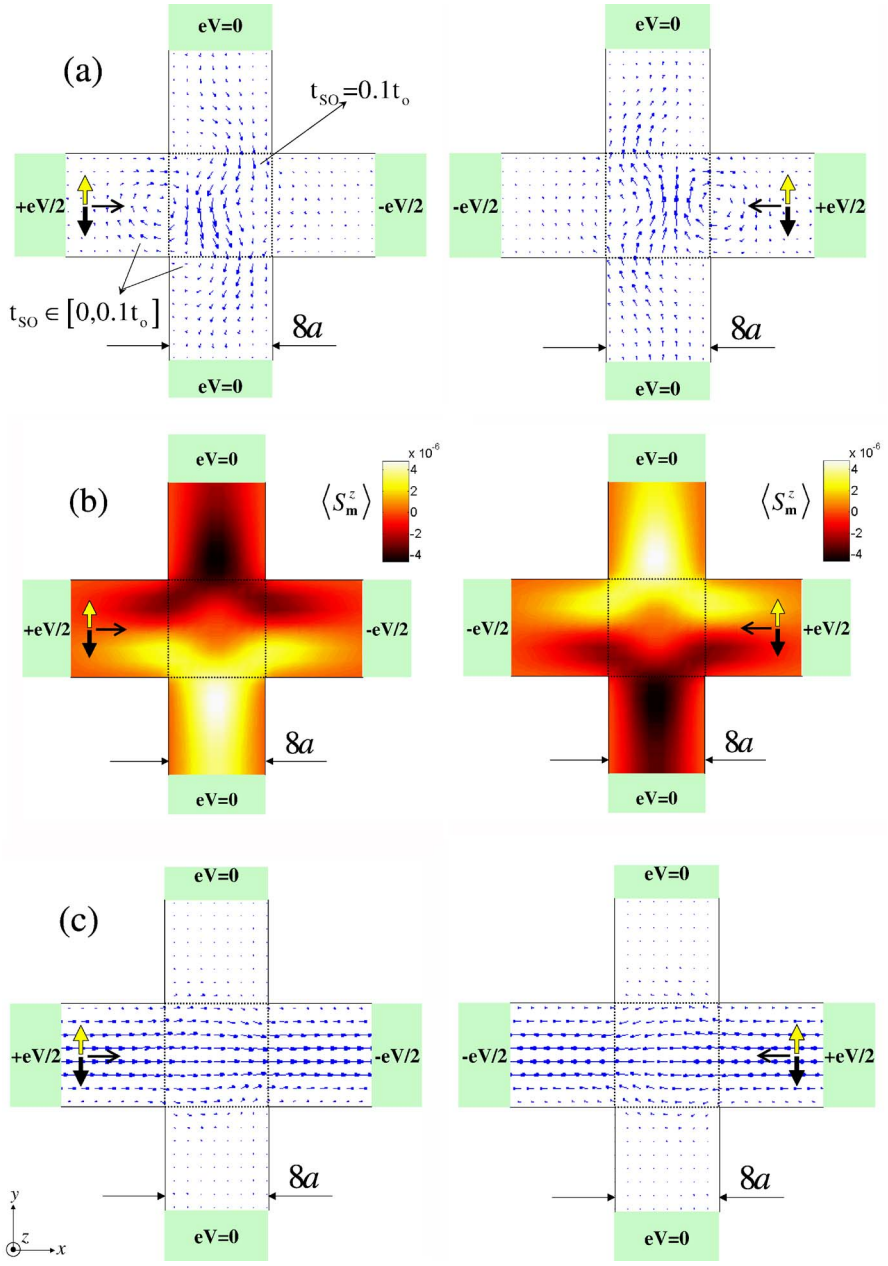

FIG. 3. (Color online) (a) The spatial distribution of nonequilibrium local spin currents $\langle \hat{J}^{S_z(\mathrm{neq})}_{\mathbf{mm}'} \rangle$ in ballistic four-terminal spin Hall bridges where the central finite-size 2DEG (of size $8a \times 8a$) with the Rashba SO coupling $t_{\mathrm{SO}}=0.1t_{\mathrm{o}}$ ($L_{\mathrm{SO}} \approx 15.7a$) is attached to four leads containing a region (adjacent to the sample) of length $8a$ within which the SO coupling is switched on adiabatically (using a linear function) from $t_{\mathrm{SO}}=0$ to $t_{\mathrm{SO}}=0.1t_{\mathrm{o}}$. Panel (b) shows the corresponding spatial profiles of the steady-state local spin density $\langle \hat{S}^z_{\mathbf{m}} \rangle$, while panel (c) plots the spatial profiles of the local charge currents $\langle \hat{J}_{\mathbf{mm}'} \rangle$ at each site. Upon reversing the bias voltage $V \rightarrow -V$ driving the linear response ($eV=10^{-3}t_{\mathrm{o}}$), spatial profiles in the left column turn into the profiles of the right column where both the total longitudinal charge current and the total transverse spin Hall current change their direction (Ref. 2).

mesoscale set by the spin precession length $L_{\mathrm{SO}} = \pi\hbar^2/2m^*\alpha = \pi t_{\mathrm{o}} a/2t_{\mathrm{SO}}$ (on which spin precesses by an angle π; i.e., the state $|\uparrow\rangle$ evolves into $|\downarrow\rangle$), will lead to a change of the sign[15] of spin Hall current as a function of the system size L/L_{SO}. Also, since the mesoscopic spin Hall effect sensitively depends on the measurement geometry,[15] the sign of the transverse spin Hall current can change when nonideal leads[17] are attached to the sample.

To highlight the mesoscopic features[35] (such as the effect of the measuring geometry and the properties of the attached probes) of the spin Hall effect in multiterminal ballistic SO coupled structure,[15] we plot in Fig. 3 the spatial profile of microscopic spin currents for the four-terminal bridge attached to the leads where Rashba SO coupling is switched on adiabatically (via a linear function) within the finite region of the leads adjacent to the 2DEG sample in the center of the

device. In this measuring setup, the reflection[59] at the interface separating zero and nonzero SO coupling regions is greatly suppressed, thereby enhancing the spin Hall current[15] [as encoded by longer arrows in the profiles of Fig. 3 when compared to Fig. 1(d)].

Since local spin current within the central region is not conserved, as manifested by the total spin current changing magnitude between different transverse cross sections (see Sec. V for total spin current profiles) separated by long distances $\gtrsim L_{\mathrm{SO}}$, the spatial profiles of the local spin current density appear not to be directly measurable.[3] However, the nonequilibrium spin density (i.e., the related spin magnetization) is a well-defined and measurable quantity.[1,2] Therefore, we plot the spatial distribution of the stationary flowing spin density $\langle \hat{S}^z_{\mathbf{m}} \rangle$ Eq. (42) in Fig. 3 to gain additional insight into the microscopic details of the spin Hall quantum transport. These pictures convincingly demonstrate how spin-$\uparrow$ and spin-$\downarrow$ densities flow in opposite transverse directions through the attached leads, without any net charge flow in the transverse direction, thereby giving rise to a *pure* transverse spin Hall current. When we reverse the direction of the longitudinal charge current (by reversing the bias voltage $V \rightarrow -V$), the transverse spin current and spin densities flip their sign, as exploited in experiments to confirm the strong signatures of the spin Hall effect.[2] The spatial profiles of the local charge currents in Fig. 3(c) also provide insight into the spin Hall effect–induced modifications of the longitudinal charge flow.[60]

Thus, in contrast to the arguments[21] suggesting the impossibility of spin Hall transport and accumulation via mechanisms driven solely by the intrinsic SO coupling terms in the effective Hamiltonian of spin-split semiconductors, Fig. 3 demonstrates that the spin Hall effect originating in ballistic multiterminal devices (without the necessity for impurity-induced effects) generates genuine nonequilibrium spin flux that can be used for spin injection and spintronics applications.[5]

To complete the microscopic picture of spin density flow, we examine in Fig. 4 the spatial profiles of the in-plane components $\langle \hat{S}^y_{\mathbf{m}} \rangle$ and $\langle \hat{S}^x_{\mathbf{m}} \rangle$ of stationary spin density which demonstrate the possibility of nonzero total spin polarization $\Sigma_{\mathbf{m}} \langle \hat{S}^y_{\mathbf{m}} \rangle \neq 0$ within *paramagnetic* ideal leads with no external or SO-coupling-induced magnetic fields. This can be understood as a consequence of the magnetoelectric effect discussed in the context of homogeneous (infinite) systems, where longitudinal charge current passing through a 2DEG orients spins along the y axis due to the presence of Rashba SO coupling.[61] In inhomogeneous systems, such spin accumulation within the 2DEG will, in turn, push the spin current (which, in contrast to the spin Hall current, carries only $\uparrow$ spins polarized along the y axis) into any normal lead attached to 2DEG due to the difference in respective spin-dependent chemical potentials.[15,29] The nonzero $\langle \hat{S}^x_{\mathbf{m}} \rangle \neq 0$ (with total polarization $\Sigma_{\mathbf{m}} \langle \hat{S}^x_{\mathbf{m}} \rangle = 0$) appearing around the lead-2DEG interface is due to the scattering at non-SO-coupled-region/SO-coupled-region boundary.

Another mesoscale-driven property of the spin Hall effect in ballistic nanostructures is its finite-size scaling being governed by the processes on the spin precession length L_{SO}: one can differentiate the "mesoscopic" regime $L \lesssim L_{\mathrm{SO}}$ where spin Hall current oscillates with increasing 2DEG size (changing sign with increasing size $L \times L$ of the 2DEG for strong enough Rashba SO coupling $t_{\mathrm{SO}} \gtrsim 0.04 t_{\mathrm{o}}$) and the "macroscopic" regime $L \gg L_{\mathrm{SO}}$ where it saturates at some average value.[15] While spatial profiles of local spin currents and spin densities are easy to interpret for $L < L_{\mathrm{SO}}$ (as in Fig. 1), Fig. 5 divulges how they become increasingly more intricate in the samples of size $L_{\mathrm{SO}} \times L_{\mathrm{SO}}$ (for which the spin Hall current reaches its maximum[15]) or in the macroscopic regime $L \gg L_{\mathrm{SO}}$ where the expectation value of spin completes many full precessions along the sample. Nevertheless, quantitative inspection of the profiles in Fig. 5 shows that the total spin Hall current exists only in the transverse leads (the sum of bond S_z-spin currents over any cross section within the longitudinal leads is equal to zero) where its magnitude and sign are identical to the terminal spin currents obtained from the Landauer-Büttiker formalism[15] (see Sec. V for quantitative comparison).

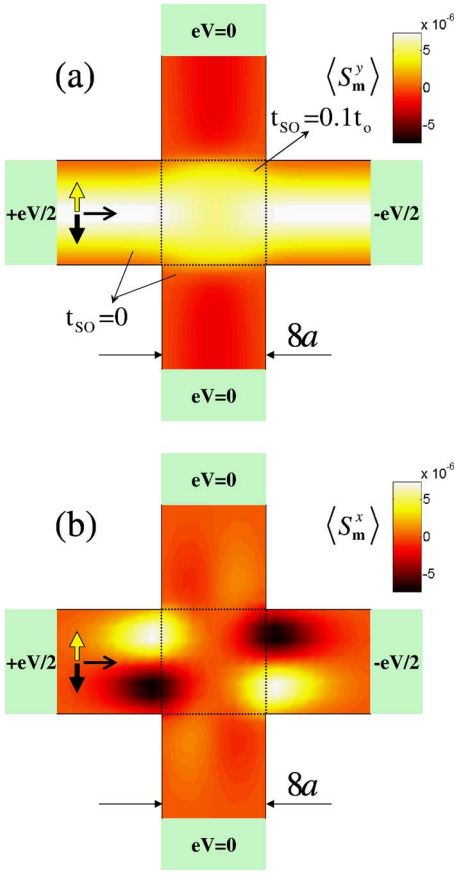

FIG. 4. (Color online) The spatial distribution of the nonequilibrium stationary flowing in-plane spin densities (a) $\langle \hat{S}^y_{\mathbf{m}} \rangle$ and (b) $\langle \hat{S}^x_{\mathbf{m}} \rangle$ in ballistic bridges consisting of four charge and spin interaction-free ($t_{\mathrm{SO}} \equiv 0$) leads attached to a finite-size 2DEG with the Rashba SO coupling $t_{\mathrm{SO}} = 0.1 t_{\mathrm{o}}$ and the corresponding spin precession length $L_{\mathrm{SO}} \approx 15.7a$. The spin densities are determined by the states within $eV = 10^{-3} t_{\mathrm{o}}$ around the Fermi energy $E_F = -3.8 t_{\mathrm{o}}$ at which longitudinal *unpolarized* linear response charge current is injected from the left lead.

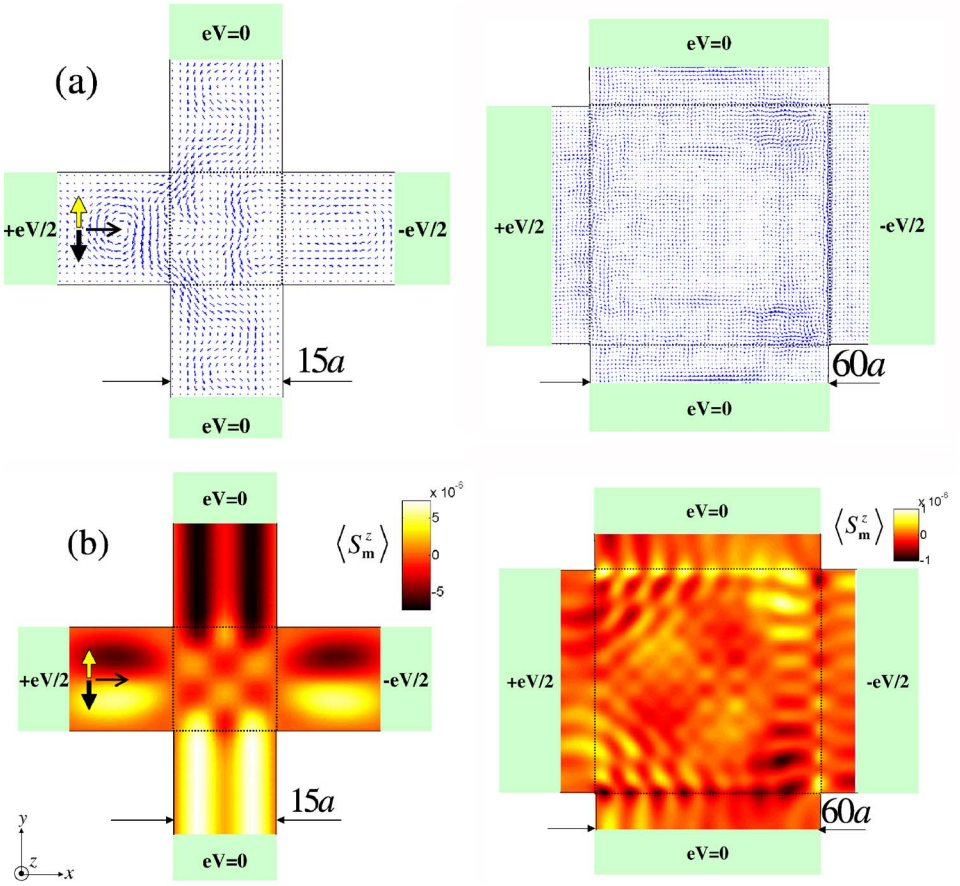

FIG. 5. (Color online) (a) The spatial distribution of the nonequilibrium local spin currents $\langle \hat{J}^{S_z(\mathrm{neq})}_{\mathbf{mm'}} \rangle$ and (b) the flowing spin density $\langle \hat{S}^z_{\mathbf{m}} \rangle$ in ballistic bridges consisting of four ideal leads ($t_{\mathrm{SO}} \equiv 0$) attached to a finite-size 2DEG with the Rashba SO coupling $t_{\mathrm{SO}}=0.1t_{\mathrm{o}}$ and the corresponding spin precession length $L_{\mathrm{SO}} \approx 15.7a$. The 2DEG central region is of the size $15a \times 15a \approx L_{\mathrm{SO}} \times L_{\mathrm{SO}}$ in the left column and $60a \times 60a$ in the right column. Note that the linear response ($eV=10^{-3}t_{\mathrm{o}}$) total transverse spin Hall current $I^{S_z}_{\mathrm{trans}}(m_y)=\Sigma_{m_x}\langle \hat{J}^{S_z}_{(m_x,m_y)(m_x,m_y+1)} \rangle$ in the leads flows along the negative y axis (i.e., from the top to the bottom transverse lead) for both device sizes.

IV. BULK vs EDGE LOCAL SPIN CURRENTS IN DISORDERED FOUR-TERMINAL RASHBA COUPLED NANOSTRUCTURES

A surprising[21] feature of the early predictions for the intrinsic spin Hall effect in hole-doped[13] or electron-doped[14] infinite homogeneous SO coupled semiconductor systems is apparent insensitivity of the spin Hall conductivity σ_{sH} to mean-free-path and relaxation rates (motivating the introduction of the term "intrinsic"[13]). This has provoked intense theoretical scrutiny[62] of the effects which spin-independent scattering off static impurities imposes on the intrinsic spin Hall current, leading to the conclusion that, in fact, $\sigma_{sH} \to 0$ vanishes[23–26] for arbitrary small disorder in any model with SO coupling linear in momentum (such as the Rashba Hamiltonian of the spin-slit 2DEG) due to accidental cancellations.[18,24,29] In the general case, where SO coupling contains higher-order momentum terms,[25,63] σ_{sH} can be resilient to sizable disorder strengths.[64] In mesoscopic Rashba spin-split 2DEG's, the value of the spin Hall *conductance* (as opposed to the bulk spin Hall *conductivity*) set in the ballistic transport regime can survive up to the rather large disorder strengths[15,17] $\Delta_{\mathrm{SO}}\tau/\hbar = 2\alpha k_F \tau/\hbar = 2(t_{\mathrm{SO}}\ell)/(t_{\mathrm{o}}a) \simeq 10^{-1}$, where ℓ is the semiclassical elastic mean free path and $\ell = v_F\tau$.

Further exploration of the disorder effects on the intrinsic spin Hall current density has led to the conjecture that macroscopic inhomogeneities facilitate spin currents[3,27] so that transverse *edge* spin current $\mathcal{J}^z_y$ would survive at the sample/electrode interfaces[28,29] even in systems where it is expected to be suppressed in the bulk.[23] However, quantitative support for the picture of edge spin Hall currents is based on analysis of semiclassical diffusive transport through a rather abstract structure, where 2DEG, infinite in the transverse direction, is attached to two massive electrodes in the longitudinal direction.[28] On the other hand, the presence of SO couplings makes the dynamics of transported spin and spin relaxation in experimentally relevant confined structures strongly dependent on the properties of their interfaces, boundaries, and the attached electrodes,[59] even for semiclassical spatial propagation of charges which carry spins evolving according to quantum dynamical laws.[65] Thus, handling of all boundary conditions relevant for experimental spin Hall bridges is essential in both quantum transport[15,17,32] and semiclassical diffusion regimes.[29]

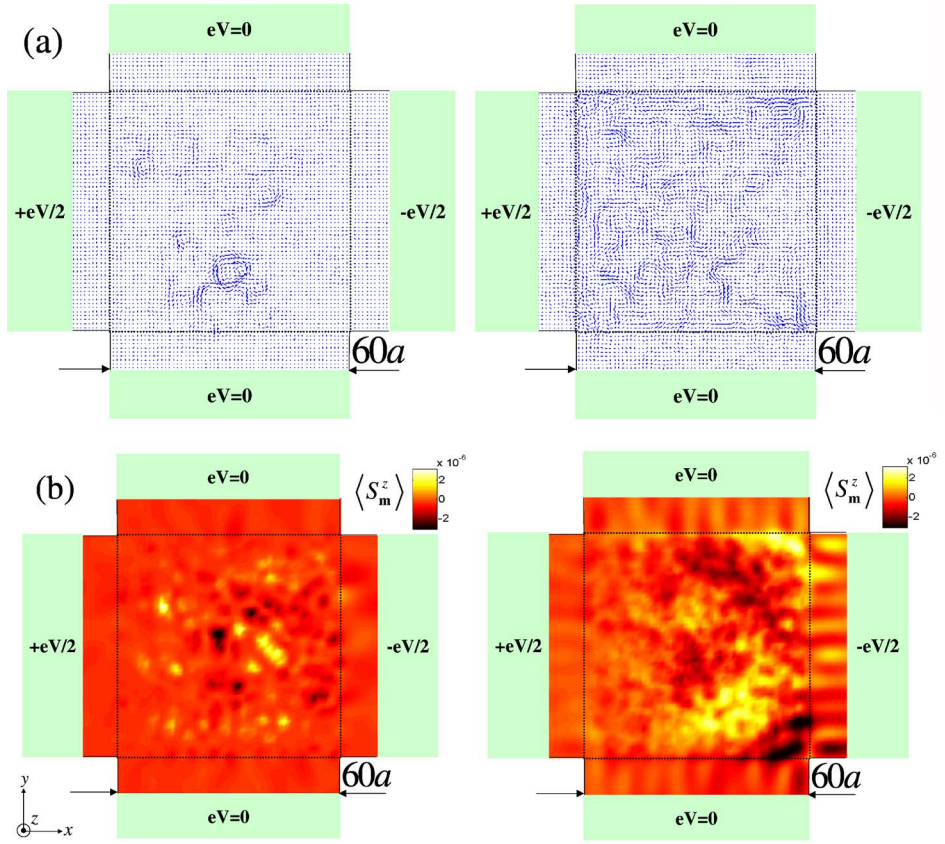

FIG. 6. (Color online) (a) The spatial distribution of the nonequilibrium local spin currents $\langle \hat{J}^{S_z(\mathrm{neq})}_{\mathbf{mm}'} \rangle$ and (b) the steady-state (flowing) spin density $\langle \hat{S}^z_{\mathbf{m}} \rangle$ in the disordered 2DEG of the size $L=60a$ with static spin-independent impurities which set the mean free path $\ell=7a$. The Rashba SO coupling within the 2DEG region is $t_{\mathrm{SO}}=0.1t_{\mathrm{o}}$ ($t_{\mathrm{SO}}\equiv 0$ in ideal leads) and the corresponding D'yakonov-Perel' spin relaxation length (Ref. 5) is $L_{\mathrm{SO}}\approx 15.7a$. The applied bias voltage $eV=10^{-3}t_{\mathrm{o}}$ between the longitudinal leads drives the linear response longitudinal charge transport (determined by the states at the Fermi energy $E_F=-3.8t_{\mathrm{o}}$) in the diffusive regime $L\gg\ell$. Panels in the left column correspond to a single sample with specific configuration of impurities, while panels in the right column show disorder-averaged profiles over an ensemble of 500 different impurity configurations.

For example, heuristic arguments based on the Keldysh formalism applied to an infinite two-terminal structure (lacking actual lateral edges) of Ref. 28 suggest that nonequilibrium spin Hall accumulation $\langle S^z_{\mathbf{m}} \rangle \neq 0$ will appear only in the four corners at the lead/2DEG interfaces (due to $\mathcal{J}^z_y \neq 0$ existing within a spin relaxation length L_{SO} wide region around such interfaces), in contrast to the Keldysh formalism applied to finite-size 2DEG in the Landauer two-terminal setup where nonzero spin accumulation (with opposite sign on the two lateral edges[1,2]) is found along the whole lateral edge both in the ballistic[9] and in the diffusive[10] transport regimes.

Within the formalism of bond spin currents of Sec. II (which represents the lattice version of the same quantity $\mathcal{J}^z_y$ analyzed in Ref. 28) these issues can be resolved through the *exact* (i.e., nonperturbative in both the disorder and SO coupling strength) evaluation of the retarded and lesser Green functions for a noninteracting particle propagating through a random potential in a finite-size multiterminal SO coupled device of a given geometry. Thus, we plot in Fig. 6 the spatial distribution of the local spin currents and spin densities for a single disordered Rashba SO coupled 2DEG, as well as their disorder averages (which are the counterpart of the macroscopic system analysis based on the diffusion equation[28]). The disorder strength is tuned to ensure the diffusive transport regime $\ell \ll L$, while the magnitude of the spin Hall current in the leads at this concentration of impurities is still about 80% of its maximum value set in the clean limit for the same four-terminal nanostructure.[15] Due to the presence of the disorder, we assume that potential landscape is $eU_{m_x}=eV/2$ for $m_x\leqslant 10$ in the left longitudinal lead, $eU_{m_x}=eV/2-eV(m_x-10)/L$ within the 2DEG sample, and $eU_{m_x}=-eV/2$ for $m_x\geqslant 70$ in the right longitudinal lead (the corresponding homogeneous electric field within the sample is sufficient to capture linear response transport properties[28,35,53]).

In this mesoscopic bridge geometry, we find that nonzero-spin fluxes are not confined to the region around 2DEG/longitudinal-lead interfaces. The conclusion based on the spatial profile of microscopic spin currents [i.e., visual distribution of arrows in Fig. 6(a)] is further corroborated in Fig. 7 by plotting one-dimensional longitudinal profiles of the bond spin currents over different transverse cross sections within the SO coupled sample and in the leads. Thus, both Figs. 6 and 7 suggest that precessing spins continues to propagate through the bulk of the diffusive Rashba SO coupled 2DEG.

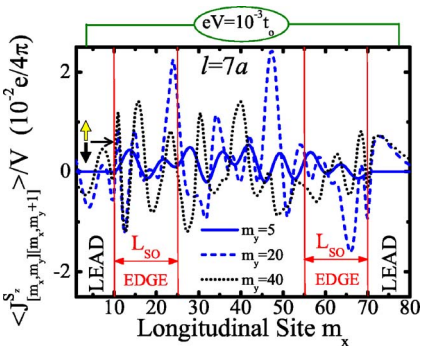

FIG. 7. (Color online) The longitudinal profile of the disorder-averaged (over 500 samples) nonequilibrium bond spin currents, whose full two-dimensional profile is shown in the right panel of Fig. 6(a), across the transverse cross sections in the ideal bottom lead ($m_y=5$) and inside the diffusive 2DEG ($m_y=20$ and $m_y=40$) with static spin-independent impurities and Rashba SO coupling $t_{SO}=0.1t_o$. Note that the length of the $m_y=5$ cross section within the bottom transverse lead is $60a$, while the length of $m_y=20$ and $m_y=40$ transverse cross sections is $80a$ ($60a$ inside the 2DEG+$10a$ within each of the two longitudinal leads). Vertical lines define the spin-relaxation-wide edges around longitudinal-lead/2DEG interfaces.

V. TOTAL vs LOCAL SPIN HALL CURRENT: LANDAUER-BÜTTIKER vs LANDAUER-KELDYSH PICTURE

The traditional charge transport experiments measure total current I and the conductance $I=GV$ relating it to the voltage drop V, rather than local current density $\mathbf{j}$ and the conductivity $\mathbf{j}=\sigma\mathbf{E}$ relating it to the externally applied electric field $\mathbf{E}$ (note also that in ballistic transport or quantum-coherent transport through a diffusive conductor conductivity ceases to exist as a local quantity[35]). Since realizations of total pure spin current have been detected experimentally in optical pump-probe experiments[66] and several theoretical schemes are proposed to detect them indirectly via various electrical measurements,[7,32,67] we focus in this section on the properties of the total spin Hall current $I^{S_z}_{\rm trans}(m_y)$ at different transverse cross sections (specified by coordinate m_y) of our four-terminal devices, as obtained from Eq. (49) by summing the corresponding bond spin currents.

As shown in Fig. 8, the total pure spin current in the transverse leads, obtained by summing the nonequilibrium bond spin currents $\langle \hat{J}^{S_z({\rm neq})}_{\mathbf{mm}'}\rangle$ over an arbitrary transverse cross section of the ideal leads (where SO coupling vanishes), flows through them in a conserved fashion, $I^{s}_{\rm trans}(m_y)=$const for any $m_y\in$ lead. However, the same summation over the transverse cross sections within the 2DEG yields a quantity which is not conserved, except on the short length scales $\ll L_{\rm SO}$. This is due to the fact that, e.g., injected eigenstate $|\uparrow\rangle$ of $\hat{\sigma}_z$ will precess in the effective magnetic field of the Rashba SO coupling (along the y axis), thereby changing the amplitude of the spin current measured with respect to the z axis as the spin quantization axis. Additional quantitative information about the microscopic details of spin fluxes is provided by Fig. 9 which plots the one-dimensional longitudinal profiles of the bond spin currents over the selected transverse

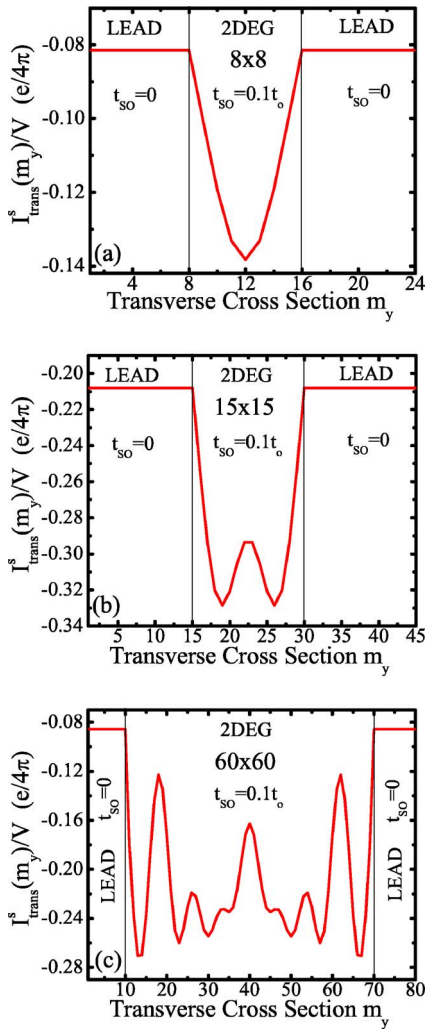

FIG. 8. (Color online) The total spin current $I^{S_z}_{\rm trans}(m_y)$ at transverse cross sections across the ideal bottom and top transverse leads (with no SO coupling) and the Rashba SO coupled 2DEG with $t_{SO}=0.1t_o$ ($L_{SO}\approx 15.7a$). The linear response longitudinal charge transport (at zero temperature) is driven by the applied bias voltage $eV=10^{-3}t_o$ between the longitudinal leads of the four-terminal structures where unpolarized electrons are injected from the left longitudinal lead at the Fermi energy $E_F=-3.8t_o$. The total pure transverse spin current in panel (a) is obtained by summing the bond spin currents in Fig. 1(d) over a cross section m_y; similarly, panels (b) and (c) correspond to such sums for the profiles in the left and right columns of Fig. 5, respectively.

cross sections (in the leads and in the 2DEG sample) cutting through the full spatial distributions of Figs. 1 and 5. Note that the sum of these longitudinal profiles yields the corresponding total spin current at the cross section m_y in Fig. 8.

The total spin currents in the leads in the linear response regime $V\to 0$ can also be calculated using the spin-dependent Landauer-Büttiker scattering formalism for spin currents in multiprobe geometries.[15,16,36] For example, the zero-temperature $T\to 0$ spin Hall conductance for a geometrically symmetric[15] four-terminal bridge with a perfectly clean Rashba 2DEG central region is given by[15,17]

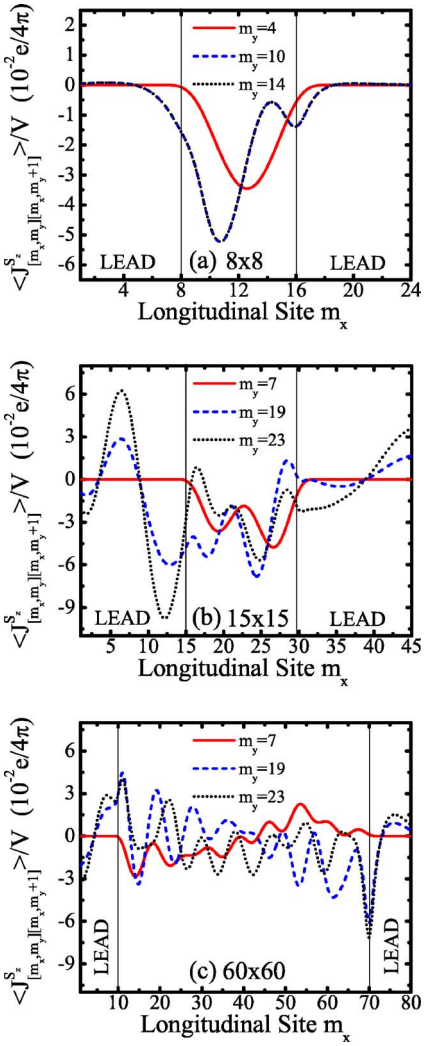

FIG. 9. (Color online) The longitudinal profile of the nonequilibrium bond spin currents along the transverse cross sections m_y in the ideal bottom lead (solid curves) and inside the SO coupled ballistic 2DEG (dashed and dotted curves). The Rashba SO coupling is $t_{\mathrm{SO}}=0.1t_{\mathrm{o}}$ ($L_{\mathrm{SO}}\approx 15.7a$) within the central 2DEG region and $t_{\mathrm{SO}}\equiv 0$ in both the longitudinal and transverse leads of the four-terminal bridge. The sum of the longitudinal profiles gives the total transverse spin Hall current in Fig. 8. Note that profile in panel (a) corresponds to the bond spin current magnitude represented by arrows in Fig. 1(d) and, similarly, panels (b) and (c) correspond to the left and right columns in Fig. 5, respectively.

$$G_{sH}^{z(\mathrm{LB})}(E_F)=\lim_{V\to 0}\frac{I_2^{S_z}}{V}=-\frac{e}{4\pi}\sum_{ij}[|\mathbf{t}_{ij,\uparrow\uparrow}^{21}(E_F)|^2+|\mathbf{t}_{ij,\uparrow\downarrow}^{21}(E_F)|^2 - |\mathbf{t}_{ij,\downarrow\uparrow}^{21}(E_F)|^2-|\mathbf{t}_{ij,\downarrow\downarrow}^{21}(E_F)|^2], \tag{53}$$

where the spin-resolved Landauer transmission matrix $\mathbf{t}^{21}$ connecting asymptotic spin-polarized scattering states at the Fermi energy E_F in the left longitudinal lead (denoted as 1) and the top transverse lead (denoted as 2) in Fig. 1 is given by

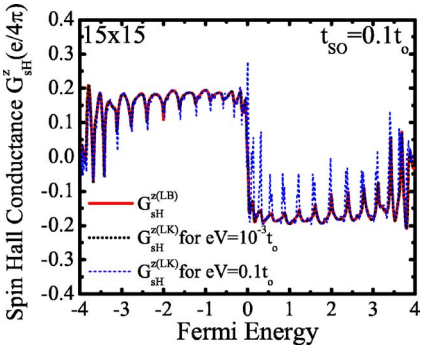

FIG. 10. (Color online) The spin Hall conductance of a Rashba SO coupled four-terminal 2DEG, obtained from the Landauer-Büttiker linear response transmission formalism as $G_{sH}^{z(\mathrm{LB})}=\lim_{V\to 0} I_2^{S_z}/V$ [where I_2^s denotes the terminal spin current in the top transverse lead in Fig. 5(a)], vs the spin Hall conductance $G_{sH}^{z(\mathrm{LK})}=I_{\mathrm{trans}}^{S_z}(m_y)/V$ obtained within the Landauer-Keldysh formalism by summing the bond spin currents over the transverse cross section in the top lead of structure in Fig. 5(a) for low bias voltage $eV=10^{-3}t_{\mathrm{o}}$ or high bias voltage $eV=0.1t_{\mathrm{o}}$ applied between the longitudinal leads. The size of the central 2DEG region is $15a\times 15a\approx L_{\mathrm{SO}}\times L_{\mathrm{SO}}$, for which the spin Hall conductance $G_{sH}^{z(\mathrm{LB})}(L,t_{\mathrm{SO}})$ reaches maximum when increasing the sample size at fixed SO coupling (Ref. 15).

$$\mathbf{t}^{21}(E_F)=\sqrt{\mathbf{\Gamma}_2(E_F)}\cdot\mathbf{G}^{21}(E_F)\cdot\sqrt{\mathbf{\Gamma}_1(E_F)}. \tag{54}$$

The sum $\Sigma_{ij}|\mathbf{t}_{ij,\sigma\sigma'}^{21}|^2$ in this Landauer-type formula goes over the orbital conducting channels[59] in the leads and gives the probability for a spin-σ' electron incident in lead 1 to be transmitted to lead 2 as a spin-σ electron. The spin quantization axis for $\uparrow,\downarrow$ is chosen to be the z axis. The submatrix $\mathbf{G}^{21}(E)$ of the retarded Green function matrix $\mathbf{G}(E)$ in Eq. (44) is composed of only those elements $G_{\mathbf{mm}',\sigma\sigma'}$ which connect the sites $\mathbf{m}$ on the edge of the sample adjacent to the left lead to the sites $\mathbf{m}'$ on the edge adjacent to the top lead. Thus, the computation of the spin-resolved transmission matrices does not require any knowledge of the elements of the retarded Green function matrix, Eq. (44), between the sites within the sample (such formulas in terms of only the retarded Green function elements between the sample edges are obtained also for the total charge currents after summing the corresponding bond charge currents[43,47]).

We demonstrate in Fig. 10 that the spin Hall conductance obtained from the Landauer-Büttiker formalism $G_{sH}^{z(\mathrm{LB})}$, Eq. (53), is almost identical to the spin Hall conductance $G_{sH}^{z(\mathrm{LK})}=I_{\mathrm{trans}}^{S_z}(m_y)/V$ obtained by summing the bond spin currents over a cross section m_y in the top transverse ideal lead, on the proviso that the applied bias voltage be small, $eV\ll E_F$, and the spin current be carried only by states at the Fermi level. This equivalence further justifies the introduction of the nonequilibrium bond spin-current formula, Eq. (32), for the z component of spin, which although not conserved in the sample, reproduces conserved terminal spin currents in the ideal leads. Note that the nonconserved nature of conventionally defined spin current within the SO coupled sample (as demonstrated by Fig. 8) is partially responsible for discrepancy between the exact Landauer-Büttiker spin

Hall conductance of the four-terminal bridge and attempts to obtain the spin Hall conductivity from the Kubo formula in exact state representation applied to finite-size samples.[68]

VI. CONCLUDING REMARKS

In conclusion, we have demonstrated how to define the bond spin current, describing the spin flux across a single bond between two sites of the lattice model of an SO coupled semiconductors, and evaluate it in terms of the Keldysh nonequilibrium Green functions for the Landauer setup where finite-size sample is attached to many semi-infinite ideal leads to form a theoretical model of experimentally accessible spin Hall bridges. Although spin current is not conserved within the SO coupled region (i.e., on the length scales comparable to the spin precession length L_{SO} on which the SO coupling manifests itself), the microscopic spin fluxes are nearly conserved on short scales. Thus, the bond spin currents make it possible to obtain their spatial distribution by following the dynamics of transported spin on the scale of the lattice spacing, $a \ll L_{\mathrm{SO}}$. Such profiles of (the lattice version of) local spin-current density, together with stationary flow profiles of physically transparent and measurable local spin densities, allow us to demonstrate microscopic details of how pure transverse spin Hall current emerges in *clean* Rashba SO coupled 2DEG through which the unpolarized longitudinal charge current flows ballistically (where electrons do not scatter off impurities and do not feel the electric field). These spatial profiles are highly dependent on whether the 2DEG size is smaller or greater than the spin precession length and can be affected by nontrivial measurement geometries, as discussed in the theory of the mesoscopic spin Hall effect.[15] The bond spin current within the bulk of the 2DEG is also resilient to weak disorder so that spin fluxes remain nonzero in the bulk of the sample and are not localized near the edges (as found in macroscopic 2DEG's[28,29]) of the diffusive mesoscopic Rashba spin-split 2DEG.

Using the spatial profiles of bond spin currents we explicitly demonstrate that nonequilibrium total spin current can be carried only by the states around the Fermi energy, while the Fermi sea contributes to local persistent spin currents which, however, do not transport any spin through a given cross section. The nanometer-scale details of the spin Hall flow in multiterminal mesoscopic (quantum-coherent) structures convincingly show that the SO couplings intrinsic to the crystal can be used to generate spin fluxes and spin accumulation and ultimately be employed to construct all-electrical spin injectors which do not require any ferromagnetic elements (thereby avoiding ferromagnet/semiconductor mismatch problems[3,5] and stray magnetic fields) and which are compatible with existing semiconductor technologies.

Finally, while the local spin current density within the sample is not conserved in the presence of SO couplings and has not been the subject of any proposed experimental measurement procedure,[3,18] here we propose to image the stationary but flowing spin densities whose detection is within the reach of present optical techniques.[41] The experimental observation of their spatial profiles in four-terminal bridges (as predicted in Figs. 3–6) within the samples would lead to deep insight into the spin dynamics within the sample which leads to pure transverse spin Hall currents outflowing from the sample into the attached external electrodes.

ACKNOWLEDGMENTS

We are grateful to İ. Adagideli, J. Inoue, N. Nagaosa, Q. Niu, M. Onoda, E. I. Rashba, and J. Sinova for enlightening discussions. Acknowledgment is made to the donors of the American Chemical Society Petroleum Research Fund for partial support of this research.

*Present address: Department of Physics, Faculty of Science, Tokyo University of Science, 1-3 Kagurazaka, Shinjuku-ku, Tokyo 162-8601, Japan.

[1] Y. K. Kato, R. C. Myers, A. C. Gossard, and D. D. Awschalom, Science **306**, 1910 (2004); V. Sih, R. C. Myers, Y. K. Kato, W. H. Lau, A. C. Gossard, and D. D. Awschalom, Nat. Phys. **1**, 31 (2005).

[2] J. Wunderlich, B. Kaestner, J. Sinova, and T. Jungwirth, Phys. Rev. Lett. **94**, 047204 (2005).

[3] E. I. Rashba, Physica E (Amsterdam) **20**, 189 (2004); J. Supercond. **18**, 137 (2005).

[4] R. Winkler, *Spin-Orbit Coupling Effects in Two-Dimensional Electron and Hole Systems* (Springer, Berlin, 2003).

[5] I. Žutić, J. Fabian, and S. Das Sarma, Rev. Mod. Phys. **76**, 323 (2004).

[6] M. I. D'yakonov and V. I. Perel', JETP Lett. **13**, 467 (1971); Phys. Lett. **35A**, 459 (1971).

[7] J. E. Hirsch, Phys. Rev. Lett. **83**, 1834 (1999); S. Zhang, *ibid.* **85**, 393 (2000).

[8] R. V. Shchelushkin and A. Brataas, Phys. Rev. B **71**, 045123 (2005).

[9] B. K. Nikolić, S. Souma, L. P. Zârbo, and J. Sinova, Phys. Rev. Lett. **95**, 046601 (2005).

[10] M. Onoda and N. Nagaosa, Phys. Rev. B **72**, 081301(R) (2005).

[11] H.-A. Engel, B. I. Halperin, and E. I. Rashba, Phys. Rev. Lett. **95**, 166605 (2005); W.-K. Tse and S. Das Sarma, cond-mat/0507149 (unpublished).

[12] B. A. Bernevig and S.-C. Zhang, cond-mat/0412550 (unpublished).

[13] S. Murakami, N. Nagaosa, and S.-C. Zhang, Science **301**, 1348 (2003); Phys. Rev. B **69**, 235206 (2004).

[14] J. Sinova, D. Culcer, Q. Niu, N. A. Sinitsyn, T. Jungwirth, and A. H. MacDonald, Phys. Rev. Lett. **92**, 126603 (2004).

[15] B. K. Nikolić, L. P. Zârbo, and S. Souma, Phys. Rev. B **72**, 075361 (2005).

[16] S. Souma and B. K. Nikolić, Phys. Rev. Lett. **94**, 106602 (2005).

[17] L. Sheng, D. N. Sheng, and C. S. Ting, Phys. Rev. Lett. **94**, 016602 (2005).

[18] S. Murakami, in *Advances in Solid State Physics* Vol. 45, edited by B. Kramer (Springer, Berlin, 2006); J. Sinova, S. Murakami,

S.-Q. Shen, and M.-S. Choi, cond-mat/0512054 (unpublished).
[19] E. I. Rashba, Phys. Rev. B **68**, 241315(R) (2003).
[20] D. Culcer, J. Sinova, N. A. Sinitsyn, T. Jungwirth, A. H. MacDonald, and Q. Niu, Phys. Rev. Lett. **93**, 046602 (2004).
[21] S. Zhang and Z. Yang, Phys. Rev. Lett. **94**, 066602 (2005).
[22] E. I. Rashba, Phys. Rev. B **70**, 161201(R) (2004).
[23] J. I. Inoue, G. E. W. Bauer, and L. W. Molenkamp, Phys. Rev. B **70**, 041303(R) (2004); R. Raimondi and P. Schwab, *ibid.* **71**, 033311 (2005); E. I. Rashba, *ibid.* **70**, 201309(R) (2004); A. Khaetskii, cond-mat/0408136 (unpublished).
[24] O. Chalaev and D. Loss, Phys. Rev. B **71**, 245318 (2005); O. V. Dimitrova, *ibid.* **71**, 245327 (2005).
[25] A. G. Mal'shukov and K. A. Chao, Phys. Rev. B **71**, 121308(R) (2005).
[26] D. N. Sheng, L. Sheng, Z. Y. Weng, and F. D. M. Haldane, Phys. Rev. B **72**, 153307 (2005); K. Nomura, J. Sinova, N. A. Sinitsyn, and A. H. MacDonald, *ibid.* **72**, 165316 (2005).
[27] A. Shekhter, M. Khodas, and A. M. Finkel'stein, Phys. Rev. B **71**, 165329 (2005).
[28] E. G. Mishchenko, A. V. Shytov, and B. I. Halperin, Phys. Rev. Lett. **93**, 226602 (2004).
[29] İ. Adagideli and G. E. W. Bauer, Phys. Rev. Lett. **95**, 256602 (2005).
[30] N. Sugimoto, S. Onoda, S. Murakami, and N. Nagaosa, cond-mat/0503475 (unpublished).
[31] P. Zhang, J. Shi, D. Xiao, and Q. Niu, cond-mat/0503505 (unpublished).
[32] E. M. Hankiewicz, L. W. Molenkamp, T. Jungwirth, and J. Sinova, Phys. Rev. B **70**, 241301(R) (2004).
[33] J. Li, L. Hu, and S.-Q. Shen, Phys. Rev. B **71**, 241305(R) (2005).
[34] M. W. Wu and J. Zhou, Phys. Rev. B **72**, 115333 (2005).
[35] H. U. Baranger and A. D. Stone, Phys. Rev. B **40**, 8169 (1989).
[36] T. P. Pareek, Phys. Rev. Lett. **92**, 076601 (2004).
[37] B. I. Halperin, Phys. Rev. B **25**, 2185 (1982).
[38] F. Gagel and K. Maschke, Phys. Rev. B **52**, 2013 (1995); **54**, 10346 (1996).
[39] A. Cresti, G. Grosso, and G. P. Parravicini, Phys. Rev. B **69**, 233313 (2004).
[40] M. A. Topinka, R. M. Westervelt, and E. J. Heller, Phys. Today **56**(12), 47 (2003).
[41] S. A. Crooker and D. L. Smith, Phys. Rev. Lett. **94**, 236601 (2005); Y. K. Kato, R. C. Myers, A. C. Gossard, and D. D. Awschalom, Appl. Phys. Lett. **87**, 022503 (2005); S. A. Crooker, M. Furis, X. Lou, C. Adelmann, D. L. Smith, C. J. Palstrøm, and P. A. Crowell, Science **309**, 2191 (2005).
[42] T. N. Todorov, J. Phys.: Condens. Matter **14**, 3049 (2002).
[43] S. Nonoyama and A. Oguri, Phys. Rev. B **57**, 8797 (1998).
[44] A. Cresti, R. Farchioni, G. Grosso, and G. P. Parravicini, Phys. Rev. B **68**, 075306 (2003).
[45] G. Metalidis and P. Bruno, Phys. Rev. B **72**, 235304 (2005).
[46] L. V. Keldysh, Sov. Phys. JETP **20**, 1018 (1965).
[47] C. Caroli, R. Combescot, P. Nozieres, and D. Saint-James, J. Phys. C **4**, 916 (1971).
[48] While the Rashba SO coupling is often ascribed to the asymmetry of the confining potential along the z axis, this mechanism alone would underestimate the value of α. The corresponding average electric field is zero for the bound states in the quantum well and becomes nonzero when the effective masses in the materials comprising the semiconductor heterostructure are different. The dominant contribution to the structure inversion asymmetry is due to differing band discontinuities at the heterostructure quantum well interface for the conduction bands calculated within the $\mathbf{k}\cdot\mathbf{p}$ model. See P. Pfeffer, Phys. Rev. B **59**, 15902 (1999).
[49] S. I. Erlingsson, J. Schliemann, and D. Loss, Phys. Rev. B **71**, 035319 (2005).
[50] A. Brataas, Y. V. Nazarov, and G. E. W. Bauer, Eur. Phys. J. B **22**, 99 (2001).
[51] J. Nitta, T. Akazaki, H. Takayanagi, and T. Enoki, Phys. Rev. Lett. **78**, 1335 (1997).
[52] T. Christensen and M. Büttiker, Europhys. Lett. **35**, 523 (1996).
[53] B. Nikolić and P. B. Allen, Phys. Rev. B **60**, 3963 (1999).
[54] L. E. Ballentine, *Quantum Mechanics: A Modern Development* (World Scientific, Singapore, 1998).
[55] A. A. Kiselev and K. W. Kim, Phys. Rev. B **71**, 153315 (2005).
[56] F. D. M. Haldane, Phys. Rev. Lett. **93**, 206602 (2004).
[57] B. K. Nikolić, L. P. Zârbo, and S. Welack, Phys. Rev. B **72**, 075335 (2005).
[58] S.-Q. Shen, Phys. Rev. Lett. **95**, 187203 (2005).
[59] B. K. Nikolić and S. Souma, Phys. Rev. B **71**, 195328 (2005).
[60] A. G. Mal'shukov, L. Y. Wang, C. S. Chu, and K. A. Chao, Phys. Rev. Lett. **95**, 146601 (2005).
[61] V. M. Edelstein, Solid State Commun. **73**, 233 (1990); A. G. Aronov, Y. B. Lyanda-Geller, and G. E. Pikus, Sov. Phys. JETP **73**, 537 (1991); J.-I. Inoue, G. E. W. Bauer, and L. W. Molenkamp, Phys. Rev. B **67**, 033104 (2003).
[62] J. Schliemann and D. Loss, Phys. Rev. B **69**, 165315 (2004).
[63] S. Murakami, Phys. Rev. B **69**, 241202(R) (2004); B. A. Bernevig and S.-C. Zhang, Phys. Rev. Lett. **95**, 016801 (2005).
[64] W. Q. Chen, Z. Y. Weng, and D. N. Sheng, Phys. Rev. Lett. **95**, 086605 (2005).
[65] C.-H. Chang, A. G. Mal'shukov, and K. A. Chao, Phys. Rev. B **70**, 245309 (2004); O. Zaitsev, D. Frustaglia, and K. Richter, Phys. Rev. Lett. **94**, 026809 (2005); Phys. Rev. B **72**, 155325 (2005).
[66] M. J. Stevens, A. L. Smirl, R. D. R. Bhat, A. Najmaie, J. E. Sipe, and H. M. van Driel, Phys. Rev. Lett. **90**, 136603 (2003).
[67] F. Meier and D. Loss, Phys. Rev. Lett. **90**, 167204 (2003); A. Di Lorenzo and Yu. V. Nazarov, *ibid.* **93**, 046601 (2004); S. I. Erlingsson and D. Loss, Phys. Rev. B **72**, 121310(R) (2005).
[68] L. Sheng, D. N. Sheng, C. S. Ting, and F. D. M. Haldane, Phys. Rev. Lett. **95**, 136602 (2005); C. P. Moca and D. C. Marinescu, Phys. Rev. B **72**, 165335 (2005).